University of Denver
Digital Commons @ DU

Electronic Theses and Dissertations | Graduate Studies

1-1-2013

Generalizable Methods for Modeling Lumbar Spine Kinematics

Craig Joseph Simons
University of Denver

Follow this and additional works at: https://digitalcommons.du.edu/etd

 Part of the Other Mechanical Engineering Commons

Recommended Citation

Simons, Craig Joseph, "Generalizable Methods for Modeling Lumbar Spine Kinematics" (2013). *Electronic Theses and Dissertations*. 605.
https://digitalcommons.du.edu/etd/605

This Thesis is brought to you for free and open access by the Graduate Studies at Digital Commons @ DU. It has been accepted for inclusion in Electronic Theses and Dissertations by an authorized administrator of Digital Commons @ DU. For more information, please contact jennifer.cox@du.edu,dig-commons@du.edu.

Generalizable Methods for Modeling Lumbar Spine Kinematics

_____

A Thesis

Presented to

the Faculty of Engineering and Computer Science

University of Denver

_____

In Partial Fulfillment

of the Requirements for the Degree

Master of Science

_____

by

Craig J. Simons

June 2013

Advisor: Bradley S. Davidson, PhD

Author: Craig J. Simons
Title: Generalizable methods for modeling lumbar spine kinematics
Advisor: Bradley S. Davidson, PhD
Degree Date: June 2013

Abstract

A more complete understanding of lumbar spine kinematics could improve diagnoses and treatment of low back pathologies and may advance the development of biomechanical models. Kinematics describes motion of the five lumbar vertebrae without consideration for the forces that cause the motion. Despite considerable attention from researchers and clinicians, lumbar spine kinematics are not fully understood because the anatomy is not accessible for direct observation and the complex governing biomechanics produce small magnitude, coupled intervertebral movements.

The overall goal of this project was to develop a descriptive model of intervertebral lumbar spine kinematics that is applicable to a generalizable subject population with diverse anthropometry. To accomplish this, a method was developed for measuring three-dimensional vertebral configuration using positional magnetic resonance imaging (MRI). The method makes use of automated vertebral registration to address time limitations in current data processing techniques and improves the ability to power experimental investigations.

Finally, a geometric model of lumbar vertebral kinematics was developed using principal component regression applied to *in vivo* vertebral measurement data across the range of flexion and extension joint motion. This principal component-based approach offers unique advantages for predicting and interpreting performance of complex systems

such as lumbar joint biomechanics because no assumptions are made regarding the governing mechanisms. This provides an opportunity to infer mechanistic characteristics about intervertebral joint kinematics and to use *in vivo* data to validate musculoskeletal models.

Acknowledgements

The work presented here would not have been possible without significant contributions from several people.

Foremost, I would like to express my sincere gratitude to my advisor, Dr. Bradley Davidson, for providing tremendous guidance and insight throughout this project. Dr. Davidson's expertise, enthusiasm, and leadership were a constant source of motivation and inspiration.

Sincere thanks to Dr. Loren Cobb, Dr. Peter Laz, Dr. Mohammad Mahoor, and Dr. Nathan Sturtevant for committing their time and effort to be involved in this project as members of my thesis committee. Through their thoughtful feedback and evaluation, each made a valuable contribution to the project.

I am grateful to several undergraduate students for their diligent assistance with data processing: Haolin Xu, Naji Foster and Angel Diaz found extra time within heavy course loads to help digitize MR images.

I am incredibly appreciative for lab mates that fostered a productive and supportive work environment. Through offering humor and perspective, precisely when needed, Stuart Currie, Brecca Gaffney, Casey Myers, and Andrea Wanamaker helped make this journey far more than an academic endeavor.

Table of Contents

List of Figures

1. Introduction

Low back pain affects a significant percentage of the population and potentially diminishes quality of life. It is reported that 70-85% of people experience back pain during their lifetime (Deyo et al. 1991; Andersson 1999). While not fully understood, mechanical pathologies including vertebral instability and soft tissue degeneration are associated with low back pain (Izzo et al. 2013; Panjabi 2006; Adams & Roughley 2006). A more complete understanding of lumbar spine kinematics may enable better diagnoses of mechanical pathologies and more detailed musculoskeletal models of the lumbar spine. However, lumbar kinematics are difficult to measure because the vertebrae are inaccessible and their motions are small, coupled, and complex.

The overall goal of this project was to gain insight into lumbar kinematics of an anthropometrically diverse population using observational and descriptive methods that impose minimal mechanistic assumptions. To accomplish this goal, the project included two main objectives:

Objective #1: Develop an efficient and reliable method for measuring vertebral position and orientation using weight-bearing magnetic resonance imaging. This method addresses time limitations in current data processing techniques and improves the ability to properly power experimental investigations.

Objective #2: Develop a descriptive model for intervertebral lumbar spine kinematics that is generalizable to an anthropometrically diverse population. The descriptive model will account for subject-specific anthropometric variation.

This thesis document is organized in the following manner. Chapter 2 presents previous methods of measuring lumbar position and orientation. Chapter 3 proposes a method to efficiently measure vertebral kinematics from weight-bearing magnetic resonance images. Chapter 4 presents an overview of modeling approaches and outlines previous investigations that modeled lumbar kinematics. Chapter 5 proposes a method to model lumbar kinematics based on an interpretable data-driven structure. Chapter 6 investigates kinematics for individual intervertebral joints and their contribution to full lumbar spine configuration. Chapter 7 presents the results and suggestions for future work.

2. Measurement of vertebral position & orientation in the lumbar spine

2.1 Introduction

The lumbar spine presents a challenging environment for measurement by comparison with most skeletal joints. Several layers of soft tissue prevent direct access to the bones and the intervertebral joint motion is subtle, consisting of small magnitude translations and rotations relative to bone size. Reported values for vertebral rotation range from 13-16 degrees per vertebra across the full range of flexion and extension motion (Pearcy et al. 1984). Methods used to measure lumbar motion range from skin surface techniques to medical imaging methods. The following provides a summary of lumbar spine anatomy and an overview of methods used to measure the vertebral position and orientation.

2.2 Lumbar Spine Anatomy

The lumbar spine transfers loads between the torso and pelvis while also enabling a large range of motion. The lumbar spine consists of five stacked bones called vertebrae located between the rib cage and the pelvis (Figure 2.1) and a spinal motion segment is composed of two adjacent vertebrae and their adjoining intervertebral disc. The vertebrae are irregular bones with large cylindrical bodies and bony processes that extend posteriorly and laterally to either side. The viscoelastic intervertebral disc separates

adjacent vertebrae and several ligaments create passive connections between neighboring vertebrae. Each vertebra is capable of three translational and three rotational degrees of freedom relative to the adjacent vertebrae. The attachments between adjacent vertebrae, formed by ligaments, muscles, intervertebral discs, and facet contact between bones prevent the vertebrae from moving independently under normal, healthy conditions. Therefore, healthy vertebral rotation and translation should be coupled (Niosi & Oxland 2004). The lumbar spine has a natural convex curvature anteriorly, called lordosis, which is thought to provide shock absorption (Adams & Hutton 1985).

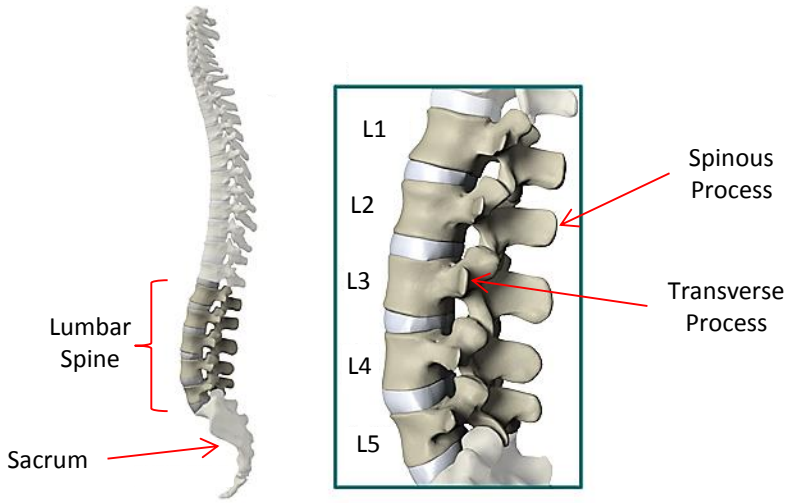

Figure 2.1: Basic lumbar spine anatomy

2.3 Lumbar Measurement Methods

Measurements can be made at the skin surface with inclinometers, goniometers, and motion capture devices to assess spinal range of motion. These measurements are clinically useful for diagnosing low back pain. However, they are limited to measuring

regional motion and do not provide information about the individual positions or rotational orientation of the vertebrae (Fritz et al. 2005; Burdett et al. 1986). Individual vertebral position and orientation can only be obtained through measurement of the vertebrae themselves. Measurements are categorized as either *in vivo* or *in vitro*. *In vivo* measurements are performed on living subjects whereas *in vitro* measurements use some portion of the original anatomy taken from a cadaveric specimen. An obvious advantage of *in vitro* measurement is that it allows for direct access to the anatomy of interest by removing obstructive tissues and bones. This enables direct position measurements at the points of interest. *In vitro* measurement also enables specific anatomical portions to be isolated and manipulated under controlled conditions, which allows specific mechanical and tissue characteristics to be characterized (Brown et al. 2002).

In vivo measurement necessarily limits access to the vertebrae but provides motion characteristics that have not been altered by dissection or loss of active muscle contribution and are classified as either invasive or noninvasive. Examples of invasive *in vivo* measurements are limited due to practical and ethical limitations/considerations. A notable example of invasive *in vivo* vertebral measurement is from Kaigle et al. (1992), which inserted bone pins through the skin and into the spinous processes of adjacent vertebrae (Figure 2.2). While this technique allows a more direct observation of vertebral motion, the study conditions may yield abnormal results due to pain and discomfort as well as increased motion resistance created by the interaction between the bone pins and the tissue at the insertion point.

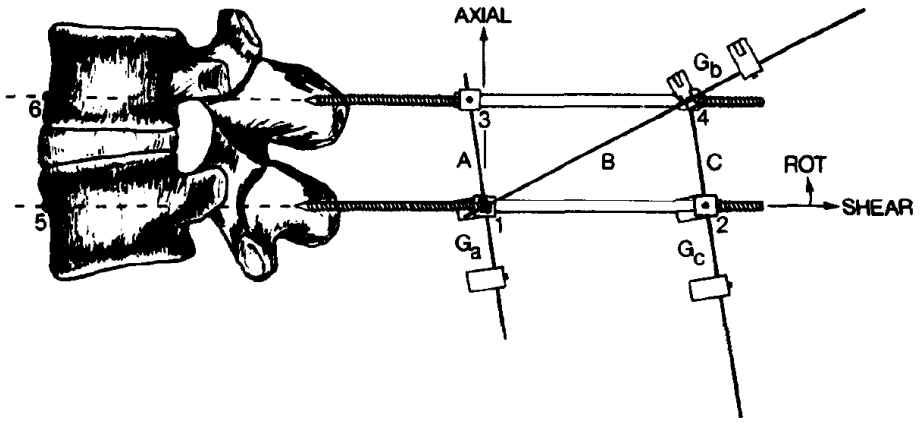

Figure 2.2: A schematic diagram of Kaigle's intervertebral motion device using bone-pins placed at the spinous processes of adjacent vertebrae. (Image taken from Kaigle et al. 1992)

The most commonly used form of noninvasive *in vivo* measurement is medical imaging. Medical imaging provides a powerful tool for spinal measurement by generating detailed images of anatomical structures located beneath the skin. Radiographic techniques, such as conventional x-ray imaging, produce images by directing a beam of electromagnetic radiation through the object of interest. The portion of the beam that is not absorbed or scattered by the object generates an exposure image on the opposite side of the object. Radiography is particularly effective for evaluating bone geometries but requires exposure to ionizing radiation, a known health risk.

Planar radiographs have been used extensively for measuring sagittal plane vertebral rotation and translation (Allbrook 1957; Pearcy & Bogduk 1988). However, limitations include image distortion effects introduced by divergence of the radiographic beam, an issue that must be corrected during data processing (Frobin et al. 1996). Fluoroscopy is a variation of the standard planar radiographic technique that enables dynamic real-time imaging by focusing a continuous x-ray beam onto a fluoroscopic screen. Although fluoroscopy presents an increased cumulative dose of radiation and

requires substantial data processing effort due to the increased volume of imaging data, this has been used in several studies measuring vertebral kinematics (Teyhen et al. 2007; Ahmadi et al. 2009).

Computed tomography (CT) and magnetic resonance imaging (MRI) provide three-dimensional data from bony and soft tissues. A significant benefit of collecting three-dimensional (3D) lumbar data is the ability to examine non-planar motion. CT uses higher doses of ionizing radiation than conventional x-ray imaging, limiting its use in elective research (Brenner & Hall 2007). While use of CT for measuring bony lumbar anatomy has been somewhat limited, the high spatial-resolution capabilities are beneficial for examining small displacements during with axial lumbar rotation (Ochia et al. 2006).

MRI uses a magnetic field to generate 3D anatomical images. A magnetic field ranging in strength from 0.3-3 Tesla is directed across the area of interest, creating magnetic polar alignment within atomic nuclei in the field. After removing the magnetic field, the magnetically aligned states return (relax) to lower energy equilibrium states and emit radio-frequency waves. Tissues with different relaxation times emit different frequencies, which allows for visual differentiation of bony and soft tissues. MR imaging has been used extensively in research to obtain 3D position and orientation of the lumbar vertebrae *in vivo*. Because conventional MRI requires image collection within a restrictive horizontal tube, participants must lie in a prone or supine position during image capture, which limits the range of motion and alters the normal direction of gravity with respect to standing postures. Fujii et al. (2007) approximated natural rotations in the prone position by building a rotating hip fixture which allowed for imaging at fixed axial rotations. However, this configuration is not able to account for gravitational effects.

Weight-bearing MRI is a modified version of conventional MRI with a non-restrictive image capture volume that addresses conventional MRI's inability to collect spine images in axial loading positions. Weight-bearing MR images can be collected while the participant is standing and under normal gravitational loading. In addition, an expanded field of view accommodates a large range of motion for most joints. However, as with conventional MRI, weight-bearing MR images are limited to static positions and participants must remain motionless during collection because movement introduces artifacts in the image. Imaging power is lower in weight-bearing MRI (0.5-0.6 Tesla) compared to conventional MRI (up to 3 Tesla), which provides an overall lower level of detail.

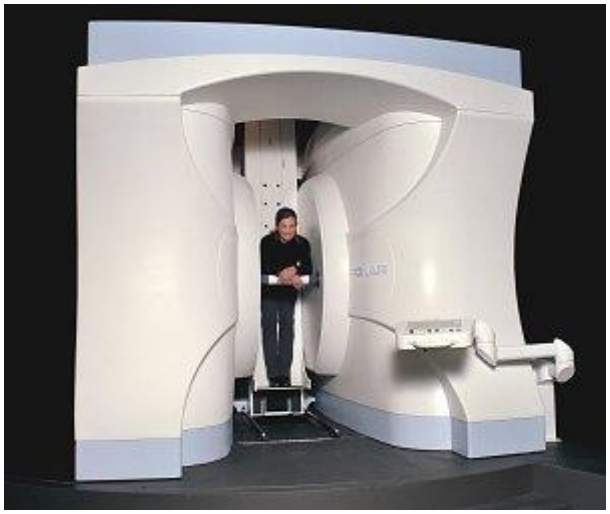

Figure 2.3: Fonar 0.6-Tesla Upright MRI scanner (Photo taken from fonar.com)

MRI provides 3D information as a series of planar image slices spanning the volume of interest. Segmentation is the process of reconstructing volumes of interest from the planar image slices. This process requires identifying the corresponding areas of interest in each image slice. Segmentation speed and accuracy are strongly influenced by

the clarity and detail available in the images. In high contrast images with well-defined boundaries, selection of the areas of interest can be automated using identification algorithms. However, vertebral segmentation is particularly challenging because the soft tissues surrounding the bone results in diminished contrast and definition near the edge of the bone. Automated segmentation algorithms have typically been implemented on MR images created from 1.5 Tesla or stronger machines (Carballido-Gamio et al. 2004; Huang et al. 2009). MR images generated by lower powered MRI devices often require region detection to be performed manually. Manual segmentation is laborious and sensitive to rater error. However, studies have confirmed the ability to reliably reconstruct vertebral bodies based on visual identification performed by skilled raters (Cargill et al. 2007). The challenge of quickly and accurately segmenting low detail MR images is a limiting factor in data analysis capabilities. Developing segmentation capabilities that are insensitive to noise is an area of active research. Schmid and Magnenat-Thalmann (2008) and Strickland et al. (2011) have both sought means for improving boundary detection methods for automated segmentation through use of shape recognition. Until these methods are refined and sufficient for low energy machines, manual segmentation is still necessary. Cargill et al. (2007) determined that manual segmentation was superior to two automated methods for their study.

Registration is an additional data processing step that is performed when two digitized geometries (vertebrae, in this case) must be combined. Registration involves spatially aligning two digitized geometries. For example, a high-detail MR scan of a bone can be registered with a lower detailed version of the same bone located in a particular position of interest. The result of the registration provides high-detail anatomical

information about the bone as it exists in the position of interest. A standard procedure currently does not exist for registering low and mid-field MR images. Methods for accomplishing registration are chosen based on the speed and accuracy requirements for the result as well as the amount of detail that is available within the registration geometries (Maintz & Viergever 1998). The iterative closest point (ICP) algorithm (Besl & McKay 1992) provides one automated method for registering two digitized volumes. The ICP algorithm operates by seeking the alignment that minimizes the mean squared error of the distance between the constituent surface points of the two objects being registered.

3. A fast, accurate, and reliable reconstruction method of the lumbar spine vertebrae using positional MRI

3.1 Introduction

Conventional magnetic resonance imaging (MRI) provides high-detail images of bone and soft-tissues, and is collected in a noninvasive manner; however, several positioning restrictions may limit the applicability of conventional MRI in orthopedic modeling. Conventional MRI requires the person to lay supine inside a cylindrical capture volume, which reorients gravity and alters the natural shape of multi-joint structures such as the spine. For example, the supine position reduces lumbar lordosis when compared to a neutral standing position (Wood et al. 1996). To approximate the normal effects of gravitational loading on the spine, some investigators have applied compressive loads to the participant while lying supine (Wisleder et al. 2001; Kimura et al. 2001; Lee et al. 2003). In addition, the cylindrical capture volume limits the range of motion of most joints. In the lumbar spine, investigations of vertebral joint mechanics are limited to axial rotations because functional sagittal plane flexion-extension or lateral bending positions are not feasible (Fujii et al. 2007; Haughton et al. 2002).

Positional MRI is a recent adaptation of conventional MRI technology that allows image collection during standing and seated postures within a capture volume that is less

restrictive than conventional MRI. Because a person can stand or sit in an open capture volume, pathologies can be viewed by physicians and researchers under natural loading (both gravitational and muscle loading), and joint biomechanics can be assessed across the functional range of motion. Soft tissue pathologies such as lumbar disc herniation are sensitive to loading conditions and torso position, which supports using positional MRI as a diagnostic tool (Zou et al. 2008). Positional MRI was recently used to characterize lumbar spine geometry during natural gravitational loading. Cargill et al. (2007) investigated changes in intervertebral position of the lumbar spine during seated flexion and extension and Meakin et al. (2008) quantified changes in lumbar curvature in response to a range of axial loads while standing.

The ability to collect images in natural weight-bearing postures with short acquisition times provides a unique opportunity to investigate *in vivo* intervertebral translation and rotation throughout a range of torso positions. These data may be used to enhance musculoskeletal models (McGill 1996), diagnose pathologies that are sensitive to loading and posture (Alyas et al. 2008; Jinkins et al. 2003), and develop motion preserving orthopedic implants (Bao et al. 1996). When coupled with efficient processing, the short acquisition times will allow researchers to power imaging and computational investigations to account for intersubject variability.

Although positional MRI can accommodate larger joint range of motion than conventional MRI, this is achieved with reduced imaging power. Positional MRI uses mid-field magnet strength (0.5-0.7 Tesla) and the large collection volume typically increases the object-to-image distance, which can result in lower image quality compared to conventional MRI collected with high-field magnets. In addition, the probability of

incurring motion artifact in an image is increased when collecting images in non-supine postures. To reduce the likelihood of participant motion and limit participant fatigue, short image acquisition times are often used with positional MRI. Protocols that use long scan times to obtain the greatest image detail possible from a mid-field magnet are impractical in relevant positions such as partial lumbar flexion.

To take full advantage of positional MRI, an accurate, reliable, and efficient reconstruction method is needed for obtaining intervertebral measurements from mid-field MR images. Past investigations have relied on manual segmentation and registration to reconstruct the vertebrae (Cargill et al. 2007). Automated segmentation methods that rely on image contrast between different tissue types are commonly used with computed tomography (CT) and high-field MRI scans. However, these are not applicable to positional MRI because of insufficient image contrast between bone and the surrounding soft tissues. Therefore, manual segmentation must be used for positional MR images. Manual segmentation is time consuming and is susceptible to boundary misidentification. Cargill et al. (2007) performed multiple segmentations and registrations for each vertebra and averaged the results across raters to reduce these errors. Although effective, performing multiple segmentations and reconstructions drastically increases processing time and precludes using large data sets to power generalizable investigations.

In this investigation, we present a semi-automated reconstruction method (manual segmentation and automated registration) specifically designed for positional MR images of the lumbar spine. Section 3.2.1 presents the reconstruction method, which expands the research capability of positional MRI in three ways. First, it provides quantifiable measurements of *in vivo* lumbar vertebral configuration with known accuracy. Second, it

introduces automated registration to reduce data processing times. Third, it uses manual segmentation techniques that are insensitive to rater error. Section 3.2.2 presents an evaluation of the reconstruction method using a criterion measurement standard. An array of manual segmentation methods are tested for accuracy and reliability with respect to the position and orientation measurements using an ovine lumbar spine specimen. We also consider the processing efficiency (speed) of each of the manual segmentation methods. Section 3.2.3 applies the reconstruction method to *in vivo* human lumbar spine data collected throughout a range of flexion-extension postures and evaluates interrater reliability.

3.2 Methods

3.2.1. *Vertebral Reconstruction Method*

The vertebral reconstruction method uses an iterative closest point (ICP) algorithm to combine two different types of T1-weighted fast spin-echo scans collected from a FONAR 0.6-Tesla Upright MRI (Fonar Corporation, Melville, NY) using a planar coil. The first type of MRI scan, the *reference scan*, was performed in a seated position. The reference scan protocol was designed to maximize image detail, but requires a longer collection time than would be sustainable while performing unstable standing postures. Posture (vertebral configuration) is irrelevant during the reference scan, so a position that is easy to maintain such as seated or supine should be selected. The second type of MRI scan, the *postural scan*, was collected in the posture of interest with a short scan time. The postural scan protocol makes use of short scan times to minimize motion artifact and participant fatigue. However, the postural scan protocol provides less detail than the

reference scan due to a larger slice thickness, increased slice interval, and fewer total slices through the anatomy (Table 3.1).

Table 3.1: MRI scan protocol for vertebral reconstruction using a FONAR 0.6-Tesla Upright scanner

	Scan Time (min:sec)	# of slices	Slice thickness (mm)	Slice interval (mm)	Field of View (cm)	Repetition Time (ms)	Echo Time (ms)
Reference Scan	5:17	20	4	4	30	610	17
Postural Scan	3:02	10	5	8	30	350	17

A reconstruction of the postural configuration with detail equivalent to the reference scan was achieved by registering each segmented vertebra from the reference scan with the corresponding segmented vertebra from the postural scan. Bone surface geometries were segmented from all scans to create three-dimensional (3D) point clouds using ScanIP (Simpleware, Exeter, UK). Each vertebra from the reference scan was registered to the corresponding postural vertebra using an ICP algorithm (Figure 3.1) that aligns the reference scan vertebra with the equivalent postural vertebra such that the distance between vertebral surface points is minimized (Besl & McKay 1992).

Prior to performing the ICP algorithm, a right-handed body-fixed coordinate system was assigned to each vertebra and sacrum from the reference scan and to the sacrum from the postural scan. These coordinate systems were assigned according to the ISB recommendation (Wu & Cavanagh 1995). This was accomplished using the 3D point clouds with SolidWorks (Dassault Systèmes, Vélizy, France) through a four-step process.

Step 1: Planar rectangles were defined tangent to the caudal and cranial endplates. The rectangular edges were positioned tangent to the anterior, posterior, and lateral edges of each endplate.

Step 2: The origin was defined at the midpoint of a line-segment connecting the center points of each rectangle. This line segment also defined the *y*-axis of the coordinate system.

Step 3: The *x*-axis was defined by a line that projects anteriorly from the coordinate system origin and intersects a line segment that joins the mid-points of the anterior edges of the caudal and cranial rectangles.

Step 4: The *z*-axis was defined as the cross product of the *x*-axis and *y*-axis.

The sacral coordinate system was defined using the same coordinate axis convention. However, only one rectangular plane located on the superior sacral endplate was defined. The coordinate system origin was positioned at the rectangle center point (Figure 3.1).

Each vertebra from the reference scan was registered to the postural scan using an ICP algorithm based on *k*-d tree point matching. The algorithm was limited to 150 iterations, and a 5% worst-point match rejection was included to improve convergence time and minimize influence from spurious data that could be introduced through MR imaging noise or segmentation error (Pulli 1999).

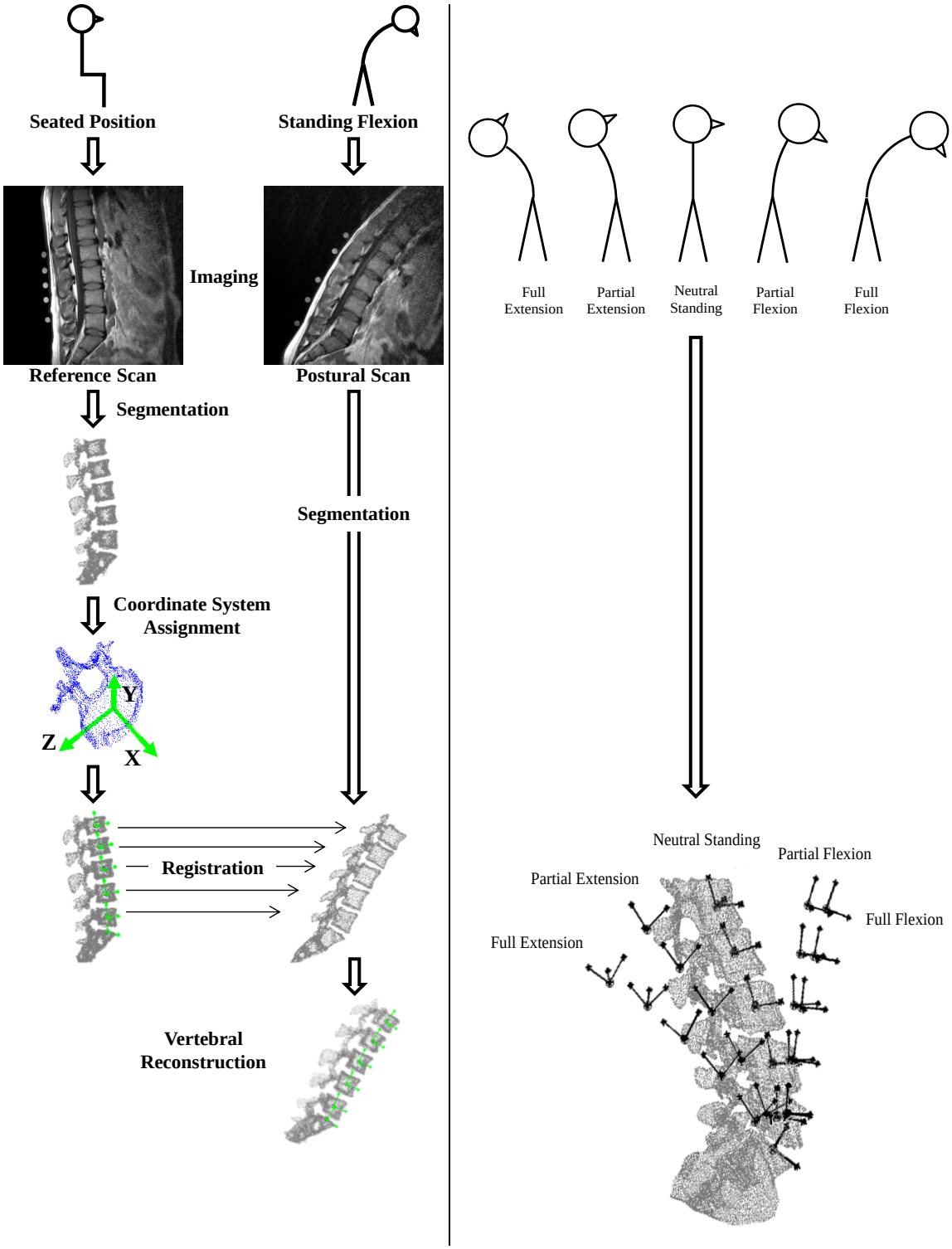

Figure 3.1: (left) Workflow for reconstructing vertebral configuration observed within positional scans using anatomic detail from the reference scan with positional MRI. (right) Vertebral reconstructions for five standing flexion and extension postures. Shown as full reconstruction in neutral standing posture and as vertebral body-fixed coordinate systems in other postures.

Two preprocessing alignment steps were used to increase the likelihood of locating a global minimum with the ICP algorithm.

Step 1: The reference scan vertebrae and sacrum were collectively translated and rotated so that the coordinate system from the reference scan sacrum was directly aligned with the coordinate system from the postural scan sacrum. This realignment of the reference scan establishes a common coordinate system for both scans and corrects for any rotational misalignments established during scan setup.

Step 2: Each reference scan vertebral point cloud was translated so that the coordinate system origin was positioned at the spatial mean of the corresponding postural scan point cloud.

One additional step was applied to the reference scan and postural scan sacra. Because the sacrum has lateral width that typically exceeds the width spanned by the imaging protocol (80mm), and because the MRI field of view cannot always capture the full length, the sacrum is not consistently represented within the MR images. As a result, each separate scan may provide different partial representations of the sacral geometry. This reduces accuracy of registration performed with the ICP algorithm by causing the algorithm to determine alignment by associating dissimilar points with one another. To eliminate inaccuracies resulting from geometric differences between sacra, the postural scan and reference scan sacral geometries were compared with respect to the sacral body-fixed coordinate systems. Dissimilar portions of both sacra were truncated so that the remaining lateral and inferior dimensions match.

ICP registration was performed after the two alignment steps and sacral geometry matching step were completed.

Alignment steps and ICP registration were implemented using Matlab (MathWorks, Natick, Massachusetts). The ICP algorithm converged after approximately 40 iterations (3-4 seconds) for all vertebrae and segmentation methods.

Following reconstruction, position and orientation of each vertebra were measured in the sacral coordinate system. Positions were represented as rectangular coordinates (x, y, z) and rotational orientations were represented by Cardan angles (α, β, γ). The first Cardan angle (α) is a rotation about the original z-axis (i.e. a rotation in the sagittal plane). The second (β) and third (γ) Cardan angles are rotations about the successively rotated x- and y-axes.

3.2.2. *Selection of Segmentation Method using In Vitro Specimen*

Manual segmentation introduces human error into the reconstructions and is the most time-consuming step in the reconstruction method. Therefore, we measured accuracy, reliability, and processing efficiency of the vertebral reconstruction method across eight manual segmentation methods using an *in vitro* ovine spine. The spine specimen included four vertebrae (T12, T13, L1, and L2) with intact intervertebral discs and partially intact musculature. To establish a criterion standard for measurement, the specimen was scanned using CT with 0.625mm thick axial slices (0.625mm gap, 1.25mm interval) from a GE HiSpeed QX/i scanner. The specimen was also scanned with a FONAR 0.6-Tesla Upright MRI using the reference and postural protocols (Table 3.1) and reconstructed using the procedure described in the previous section. The ovine specimen was vacuum-sealed in heavy-gauge plastic and kept near freezing throughout the imaging procedures to maintain fixed intervertebral positions during all scans for comparison.

The eight manual segmentation methods differed according to the continuity of the boundary assigned to segmented structures (vertebral body, spinous process, or transverse process) from each MR slice (Figure 3.2). The continuity conditions ranged from selecting the "corner points" of these structures plus one additional point on the boundary between corner points to selecting a continuous boundary. For each of the seven point selection techniques, points were placed along the boundary with consistent spacing between points. In ScanIP, the point-based segmentation methods produced point clouds consisting of only the points selected from each image slice. The continuous boundary condition in ScanIP generated an interpolated surface.

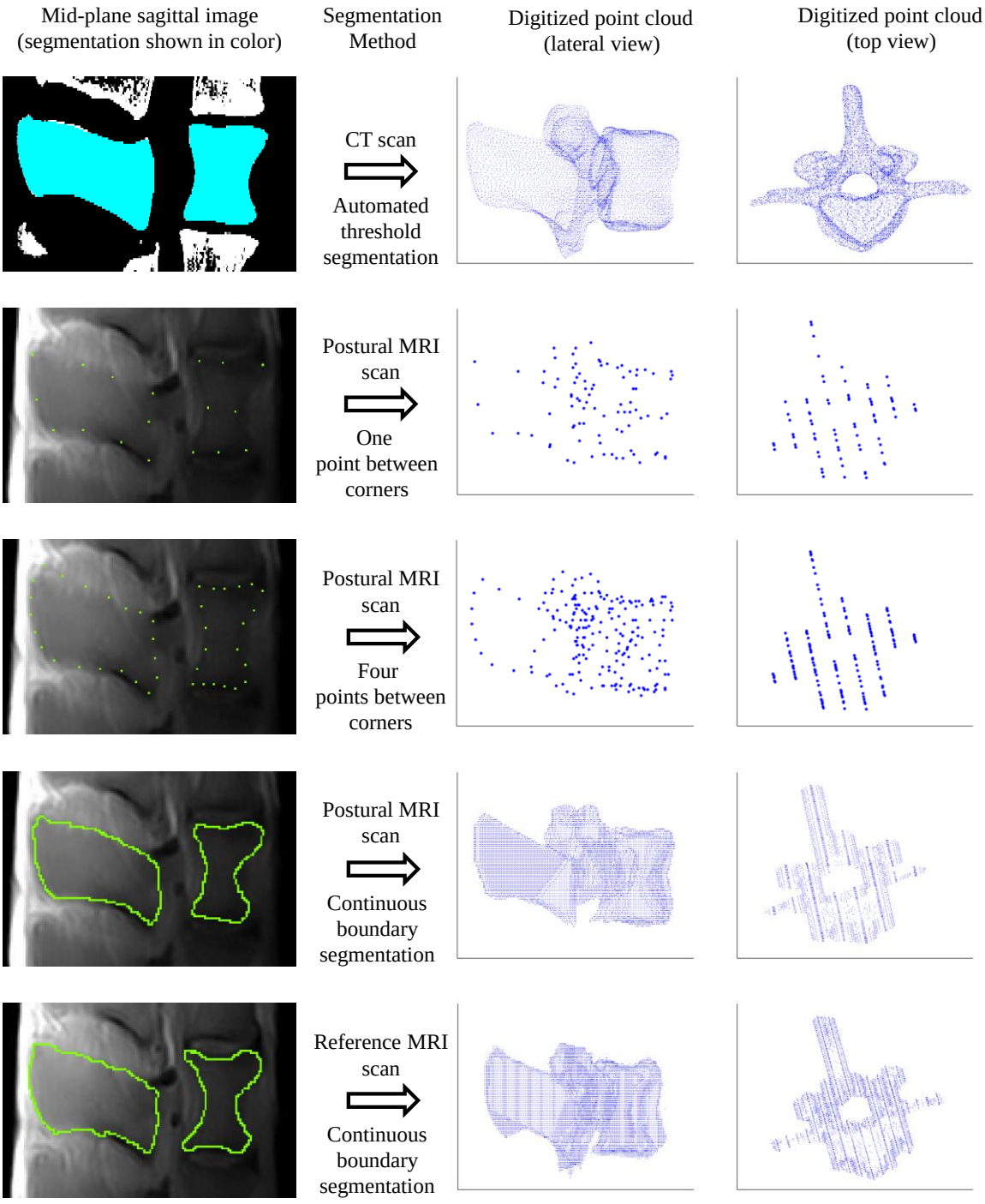

Figure 3.2: Segmentation of a mid-plane sagittal slice of an ovine L1 vertebra (left) and the digitized point clouds that are generated from the segmentation (right and far right). Position and orientation of the sagittal MR slices relative to the anatomy are visible as distinct lines in the top view for the "point" segmentation methods.

Because the ovine specimen maintained a fixed vertebral configuration throughout all scans, a postural configuration was simulated by translating and rotating each vertebral point cloud from the reference scan prior to performing reconstruction. The simulated geometry (+80 mm along the *x*-axis, -50 mm along the *y*-axis, and 45 degrees about the *z*-axis) was equivalent to the typical configuration between L1 and the sacrum in a human performing extreme lumbar flexion. Reconstruction was performed on the T13, L1, and L2 vertebrae. Position and orientation of the T13 and L1 vertebrae were expressed in the L2 coordinate system because the ovine specimen did not include a sacrum. The postural scans were segmented using all eight of the segmentation methods performed by three different raters (CS, HX, NF), and provided 27 total sets of postural point clouds. The reference scans were segmented using only the continuous boundary method.

Accuracy, reliability, and efficiency were quantified for reconstructions performed using each of the eight manual segmentation methods. Accuracy was quantified by the measurement error, or differences in vertebral translation and orientation measured on the CT data (criterion standard) and the MRI reconstruction. Measurements for both vertebrae (T13 and L1) were pooled for analysis. Interrater reliability was quantified based on the standard deviation of the measurement error from all reconstructions. Processing efficiency was quantified by the time taken to complete the segmentation.

3.2.3. *Reliability of Reconstructions from In Vivo Human Participants*

Because a criterion standard was not available when scanning and measuring *in vivo* human participants, error cannot be assessed. However, sensitivity of the reconstruction measurements to manual segmentation performed by different raters can be evaluated. Positional MR images were collected from three participants (2 males, 1 female, 31.3±9.5 years old) with no history of low back pain or injury. Each participant provided informed consent in accordance with the University of Denver Institutional Review Board. Each participant performed a sitting reference scan and five standing postural scans: neutral standing, maximal lumbar flexion, partial lumbar flexion, maximal lumbar extension, and partial lumbar extension. All scans were collected with a FONAR 0.6-Tesla Upright scanner according to the imaging protocols in Table 3.1.

Each MR image was manually segmented by three researchers (CS, HX, NF). All images (postural scans and reference scans) were segmented using the continuous boundary method. Each researcher segmented 75 vertebrae (3 participants, 5 positions), which provided 225 vertebrae for analysis.

Interrater reliability of reconstructed vertebral position and orientation was assessed by using the intraclass correlation coefficient (ICC) model (2,1). The dependent variables were rectangular positions (x, y, z) and Cardan angles (α, β, γ) of each vertebra with respect to the sacral coordinate system. To calculate ICC model results, mixed-model analysis of variance (ANOVA) with fixed effect of rater and random effect of vertebra were calculated. Mean square error, between subjects mean square, and between

raters mean square were taken from the ANOVA tables to calculate ICCs (Portney & Watkins 2000).

3.3 Results

Reconstruction error was calculated using the difference between MRI and CT measurements from reconstructions of the ovine spine in simulated flexion. Measurement errors were averaged across T13 and L1 vertebrae and all three researchers (Figure 3.3). Translational reconstruction error ranged from 0.68 mm to 1.6 mm and rotational reconstruction error ranged from 0.28 degrees to 2.6 degrees across the eight segmentation methods. The smallest error in the *z*-direction was 0.98 mm, achieved with the 4-intermediate point segmentation method. The lowest *x*-position error was 0.68 mm, achieved with 8-intermediate point segmentation. The lowest *y*-position error was 0.91 mm, achieved with continuous boundary segmentation. The lowest α-angle reconstruction error was 0.28 degrees, achieved with 3-intermediate point segmentation. The lowest β-angle error was 1.19 degrees, achieved with 4-intermediate point segmentation. The lowest γ-angle error was 0.14 degrees, achieved with 6-intermediate point segmentation.

The fastest segmentation time was recorded for the two intermediate-points technique, which required 5.8±3.0 minutes and yielded point clouds comprised of 109-127 points (Figure 3.4). The longest average segmentation time was recorded for the 10 intermediate-points technique, requiring 15.0±5.0 minutes on average and yielded point clouds comprised of 359-419 points. Continuous boundary segmentation required 12.1±3.4 minutes. Segmentation using the 6-, 8-, and 10-intermediate point methods requires longer segmentation time than continuous boundary segmentation.

ICCs indicated high interrater reliability for sagittal plane positions, *x* (ICC= 0.99) and *y* (0.99), but poor reliability for the *z* (0.26) position. ICCs indicated good interrater reliability for the sagittal plane rotation, α (0.97), but poor reliability for second and third rotations, β (0.18) and γ (0.26).

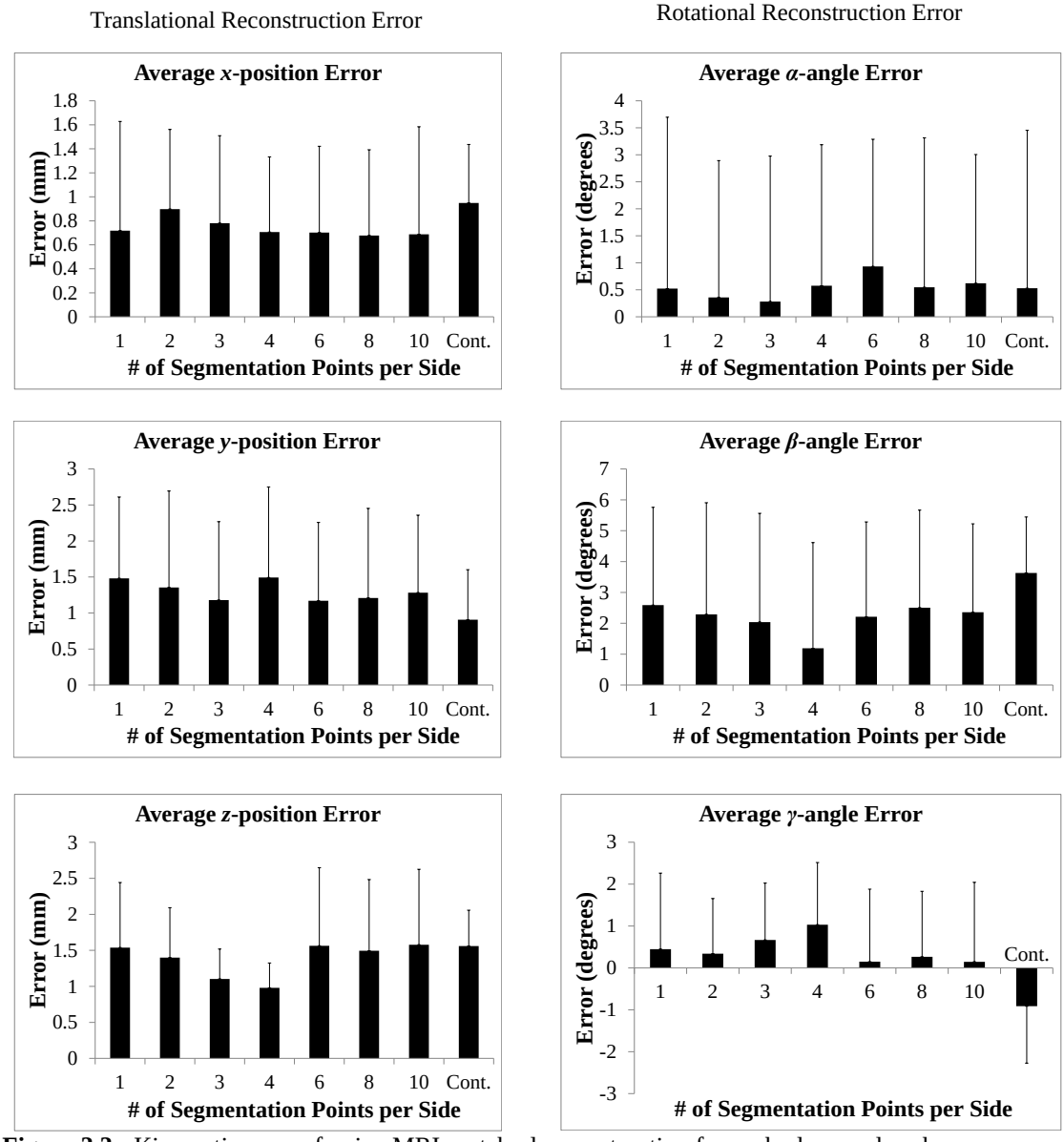

Figure 3.3: Kinematic error of ovine MRI vertebral reconstruction for each plane and each segmentation method. Reconstruction error is determined relative to a criterion standard, which was established by CT measurements. Error bars indicate one standard deviation.

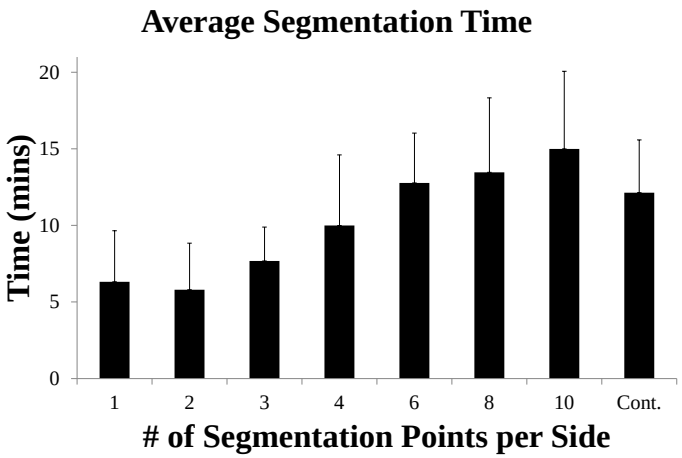

Figure 3.4: Time required to complete segmentation using each segmentation method. Results indicate average time per ovine vertebra for two ovine vertebrae (T13 and L1) segmented across three raters. Error bars indicate one standard deviation.

3.4 Discussion

The goal of this investigation was to evaluate a novel vertebral reconstruction method used to measure *in vivo* intervertebral configuration with positional MRI. This method of reconstruction addresses inherent limitations in the imaging that prevent automated segmentation methods. The vertebral reconstruction method combined two distinct positional MR scan types within a systematic and semi-automated reconstruction and demonstrated promising results. Reconstruction accuracy based on a criterion standard was within 1mm for sagittal plane positions (x, y) and 1.5mm for lateral (z) positions. Accuracy of sagittal plane rotation (α) was within 1 degree. Segmentation times were approximately 12 minutes per vertebra and registration were less than 10 seconds per vertebra. Reliability of *in vivo* reconstructions was high for sagittal plane positions and rotations but low for out of plane (lateral) positions and rotations.

The accuracy evaluation of the reconstructions from the mid-field positional MRI demonstrated promising results when compared with intervertebral measurements from

conventional imaging. For example, Lim et al. (1997) reported 3D vertebral measurement accuracy of ±1.0 mm and ±1.0 degrees using CT scans (1.0 mm x 0.43mm x 0.43 mm voxel size). More recently, Ochia et al. (2006) used a volumetric reconstruction method to evaluate lumbar axial rotation with CT scans, and reported measurement error less than 0.1 mm and 0.2 deg. We found only one comparable study that used positional MRI to perform quantitative intervertebral measurements. Cargill et al. (2007) used positional MRI for vertebral reconstruction, but no criterion standard was available to assess the measurement accuracy. In addition, a direct comparison was difficult because the measurements were presented as subject-specific intervertebral angles during various postures. Reconstruction accuracy can be influenced by specific bone geometry (Draper et al. 2008); therefore, we compared these results only to intervertebral reconstructions.

The accuracy evaluation performed using ovine vertebrae provides a conservative accuracy estimate for measurements using human vertebrae, and the method should be capable of better accuracy in human imaging. Human and ovine vertebrae are geometrically similar, but ovine vertebral bodies have a smaller lateral dimension than human lumbar vertebrae (Wilke et al. 1997). This resulted in fewer MR slices intersecting each ovine vertebra and less geometric data available from the ovine specimens for performing the registration. Also, with fewer segmentation points, effects from inaccurate point placements were likely magnified. Note, however, that an *in vitro* specimen is not susceptible to motion artifact and the specimen can be consistently positioned relative to the coil and magnetic field isocenter.

Measurement accuracy based on MR images is affected by several data collection parameters such as magnetic-field homogeneity, tissue characteristics, and location of the

anatomy relative to magnetic field isocenter. Therefore, images collected from the same scanner with the same protocol can vary in clarity. In our evaluation, we neglected any imaging error and assumed all measurement error was the result of the reconstruction method, which is a conservative evaluation of the reconstruction method. A direct evaluation of the imaging error could be performed using an MR phantom with multiple articulating vertebral segments.

Continuous boundary segmentation provided the best combination of efficiency, reliability, and accuracy and was chosen as the segmentation method to evaluate *in vivo* reliability. Error variance was higher with the intermediate-point segmentation methods compared to continuous boundary segmentation, which indicated that continuous boundary segmentation has higher reliability when segmentation is performed by multiple raters. The continuous boundary segmentation was faster than 6-, 8-, and 10-intermediate point segmentation methods. This likely occurred because continuous boundary segmentation can be performed by selecting fewer than six intermediate points per side to create a continuous-boundary spline curve. Also, with continuous boundary segmentation, no additional time is required to achieve consistent point spacing.

For the current study, MRI scan protocols were chosen to maximize reliability in the sagittal plane, but at the expense of lateral reliability. Short scan times are required during static postures to prevent participant fatigue. Therefore, MR images were collected with large slice intervals and were limited to single planar orientation (sagittal). The lack of lateral anatomic data limits reliability of measurements along the *z*-axis, which is reflected in the ICC scores. However, low lateral-position reliability may be acceptable if the primary motion of interest is sagittal plane flexion-extension because

minimal lateral displacement would be expected. Furthermore, low data variance, which is expected for lateral vertebral displacement during flexion-extension motions, will result in lower ICCs (Portney & Watkins 2000). ICCs are a ratio between actual model variance and total variance (model + error), and low model variance magnifies the effect of the error. Reliability of the lateral measurements may be improved if sagittal and coronal plane images were collected within a single scan, but this would increase scan time. In addition, the sacrum is susceptible to low lateral reliability because it is difficult to distinguish the boundary between the sacrum and the ilia, and may result in segmentation error.

This reconstruction method provides the efficiency needed to construct large datasets and power investigations that rely on population variance. Cargill et al. (2007), which used manual segmentation and manual registration, indicated that data processing times were a limiting factor when performing vertebral reconstructions from positional MRI. Although manual segmentation is necessary with mid-field MRI, our evaluation of segmentation methods indicates that accurate results can be achieved using a relatively fast segmentation method. In addition, high interrater reliability indicates that data processing can be distributed to multiple trained personnel, and can reduce the overall processing time. The automated registration with ICP significantly reduces data processing times when compared with manual registration, and offers a systematic process to follow.

In conclusion, this vertebral reconstruction method provides a systematic approach with accuracy, reliability, and efficiency. A primary advantage of the method is its use of positional MRI, which provides proper orientation of gravity and a large range

of motion without exposing the participants to ionizing radiation. The data processing steps are robust to user error and will provide efficient construction of large data sets. This approach advances current reconstruction methods, and will provide a useful tool to develop and validate biomechanical models of lumbar spine.

4. Modeling lumbar kinematics

4.1 Introduction

A more accurate description of *in vivo* lumbar kinematics could improve and help validate biomechanical models and clinical diagnoses related to spinal instability. An alternative to directly measuring lumbar kinematics is to develop models for predicting and evaluating kinematics. The goal of modeling is to determine a relationship between a set of input variables and a set of output variables. Regarding lumbar kinematics, a predictive model would create a relationship between easily measured subject-specific data and the vertebral locations and orientations.

For modeling performance of complex biomechanical performance such as lumbar kinematics, significant challenges result from overdetermined systems and coupled interaction relationships between input and output variables. As a result, modelers typically must choose whether to impose simplifying assumptions that reduce complexity at the potential expense of accuracy, or attempt to incorporate full complexity at the risk of reduced interpretability and greater potential for inaccurate assumptions. In acknowledging this complexity/accuracy dilemma, Full and Koditschek (1999) suggest that modelers must choose to create either templates or anchors. Templates provide the simplest possible representation of a system to offer insight into basic performance whereas anchors strive for complete mechanistic representation to achieve the most

accurate model performance. In the spectrum of model complexity, many biomechanical models of lumbar spine would qualify as templates, which offer simplified representations of joint performance, or hybrid anchors that model performance of a particular characteristic very accurately but do not attempt account for the full range of system behavior. Wagner et al. (2012) provides a template for evaluating optimal lordosis for maintaining spinal stability. The model constrains spinal stability to the sagittal plane and assumes a single degree of freedom at each intervertebral joint. This assumption allows for evaluation of an otherwise statically indeterminate system. By comparison, Meakin et al. (2008) offers one example of a hybrid anchor model of lumbar biomechanics by creating an active shape model of lumbar lordosis to evaluate common modes of variation in response to axial loads. This model examines a narrow range of kinematic performance but in doing so, acknowledges the inherent limitations of previous investigations that do not account for population variance or intervertebral configuration when describing lordosis. The shape model makes use of principal component analysis to identify the most significant characteristics for system performance, reducing model complexity by disregarding insignificant factors.

Breiman (2001) defines two distinct approaches to statistical modeling: data modeling and algorithmic modeling. Data modeling assumes that stochastic output variables are related to their predictor variables through an unknown process. Model development involves using data to estimate the parameters that govern the unknown process, often relying upon regression methods. Data-driven models are validated with goodness of fit tests and residual examination. Algorithmic models are unconcerned with estimating the underlying physical process. Rather, algorithmic models seek a

relationship that maps known measurement and response variables, independent of the physical process. The following is a summary of statistical models used to predict biomechanical motion.

4.2 Data Modeling

Most predictive kinematic models from past investigations have used a data-driven model. For predicting spinal kinematics, these models frequently use nonlinear regressive techniques to determine the relationship between accessible landmarks and vertebral position. Two similar investigations used planar radiographs to determine vertebral position and nonlinear regression to establish the relationship between skin markers located over the lumbar posterior processes and vertebral position measured on the radiographic images (Chiou et al. 1996; Lee et al. 1995).

Sicard and Gagnon (1993) used a different data modeling approach to achieve similar goals, predict lumbar position. A series of skin markers were used to establish the skin profile curvature while lateral radiographs again provided the vertebral position. The study used multiple regression-based transformations to map skin profile curvature to vertebral position. The underlying premise was that a series of rotations and transformations could characterize the relationship between curvature measured directly on the surface of the back and the underlying vertebral positions.

Chu et al. (2003) modeled kinematic body segments using a method of principal curves to determine the central axes of body-segment volumes obtained through motion capture video of human activity. Principal curves, and other principal component-based methods have demonstrated merit for applications to kinematic modeling techniques despite sparse prior use.

4.3 Algorithmic Modeling

Algorithmic modeling is consistent with a machine learning approach to prediction in which empirical measurements are mapped to the desired outcome variable using known data. In algorithmic modeling, the ability of an algorithm to make accurate predictions should improve with greater data experience. Furthermore, a more representative data set should yield greater predictive generalizability.

Algorithmic models have more frequently been used for classification tasks rather than regression tasks within biomechanics. At least one study used several statistical algorithms (Mixture of Gaussians, Hidden Markov Models, Switching Linear Dynamic Systems) and assessed their ability to classify human motion as natural or unnatural (Ren et al. 2005). Classification algorithms have also been successfully implemented for the sake of identifying and categorizing skeletal abnormalities. For instance, an artificial neural network demonstrated effectiveness when classifying different types of spinal deformities based on curvature pattern recognition. However, this investigation did not attempt to make any lumbar motion predictions (Lin 2008).

To our knowledge, only one investigation has used algorithmic models in a regressive framework to predict lumbar kinematics. Ma et al. (2008) used a Bayesian belief network to make kinematic predictions on the neutral position of a person's lumbar vertebral positions based on the fully flexed positions. The model structure uses probabilistic inference to generate sequential predictions with high reported accuracy. However, one limitation of this study is that model validation was based on comparisons of a particular subject at the starting point to the same subject in the neutral position. As such, it is unclear how generalizable the model is.

Meakin et al. presents an algorithmic approach by using an active shape model for lumbar lordosis but the model is limited to the neutral standing configuration, which limits applicability to broader kinematic performance. Fitzpatrick et al. (2011) is an example of an investigation that uses an algorithmic approach applied to patellofemoral joint mechanics. This study incorporates both mechanistic complexity and anthropometric variance as model input parameters and makes use of a combination of principal component analysis and probabilistic techniques to provide a thorough description of patellofemoral joint performance and sensitivity factors. However, no similar model has been developed for lumbar kinematics.

5. A description of lumbar intervertebral configuration using principal component-based manifolds

5.1 Introduction

Despite considerable attention from researchers and clinicians, lumbar vertebral joint biomechanics are not fully understood. For example, no consensus definition exists regarding precisely what distinguishes healthy and pathological lumbar kinematics (Izzo et al. 2013; Leone et al. 2007). Similarly, there is a deficit in understanding the kinematic contributions of the surrounding tissues and how these are related to pathology (Legaspi & Edmond 2007; Panjabi 2003). This deficit leads to disagreement about diagnoses and treatment methods for pathological and/or degenerative conditions (Mulholland 2008; Galbusera et al. 2008).

In comparison with many skeletal joints, efforts to understand lumbar intervertebral biomechanics have been hindered by musculoskeletal complexity and anatomy that is difficult to measure during relevant movements and configurations. The lumbar vertebrae are surrounded by several layers of soft tissue, which prevents direct access for measurement and observation. Noninvasive measurements recorded at the skin surface cannot distinguish compound intervertebral joint movements (Burdett et al. 1986;

Zhang & Xiong 2003). Therefore, many investigations use *in vitro* specimens or medical imaging technology such as magnetic resonance imaging (MRI) and computed tomography (CT) to study intervertebral biomechanics. *In vitro* specimens provide direct access to the vertebrae through tissue removal, but because this alters the natural anatomic constraints and applied loads interpretability is limited. Medical imaging technology allows *in vivo* vertebral observations but the image capture volume typically restricts joint range of motion and requires that the subject be supine, which reorients gravity and alters vertebral configuration (Fujii et al. 2007; Meakin et al. 2008).

Researchers frequently answer their hypotheses using musculoskeletal models. Musculoskeletal models provide a convenient alternative for evaluating biomechanical responses to a variety of input conditions but complexity dictates that intervertebral kinematics are often simplified as a series of one or more hinge or spherical joints within models. For example, de Zee et al. (2007)models each lumbar intervertebral joint as a three degree of freedom spherical joint and Christophy (2012) and Simonidis (2007) apply constraints that reduce 30 initial degrees of freedom to three independent degrees of freedom. Joint mechanics are then approximated at each vertebral level by assuming equivalent distributions across all joints. Although convenient, these simplified joint representations cannot fully account for the complex anatomic constraints provided by the surrounding passive tissues such as the discs, facets, and ligaments (Arjmand et al. 2007). However, these same anatomic complexities inhibit the ability to model their effects on kinematic constraints.

An alternative approach to model correct lumbar spine kinematics may be to develop phenomenological constraints for vertebral motion based on *in vivo* kinematic

measurements. Phenomenological models make use of empirical data and employ an algorithmic approach to determine the relationship between predictor variables and response variables. This approach is particularly beneficial for modeling complex systems such as lumbar spine kinematics because it does not require modelers to attempt to replicate the governing mechanics within their models. Although several investigations have used empirical *in vivo* data to drive their lumbar kinematics models, a descriptive generalizable model has not yet been fully realized. Ma et al. (2008) developed a Bayesian belief network based on superficial skin markers to predict vertebral positions measured from radiographic images. However, the study population was homogeneous and the validation process does not demonstrate generalizable predictive accuracy.

The long-term goal of this research is to create a data-based phenomenological model of lumbar intervertebral kinematics that can be used to predict subject specific vertebral configuration throughout the full range of joint motion for lumbar vertebrae. As an initial step toward this goal, the objective of this investigation is to examine whether sagittal plane vertebral translation and rotation can be described using anthropometrically scaled ellipsoid manifolds parameterized using principal component regression. By accounting for anthropometry, a foundation is established to include subject-specific geometric constraints and apply this approach to individual musculoskeletal models.

5.2 Methods

Positional magnetic resonance imaging (MRI) data was collected from 10 participants (6 men, 4 women, 30.9±6.5 years old) using a FONAR 0.6-Tesla Upright scanner. Scans were captured in six standing flexion and extension postures (full extension, partial extension, neutral standing, 1/3 flexion, 2/3 flexion, full flexion).

Digitized three-dimensional reconstructions of the lumbar vertebrae and sacrum were created for each MR scan and body-fixed coordinate systems were assigned to each vertebra and sacrum. The coordinate systems provided measurements for rectangular position (x,y,z) and angular rotation (α,β,γ) of each vertebra relative to the sacrum (Fig. 5.1). Rotation was measured using Cardan angles and the first rotation, α, was about the lateral axis (z-axis). For this investigation, vertebral modeling is limited to geometric descriptions of sagittal plane position (x,y) and rotation relative to anteroposterior position (α,x) for each vertebra.

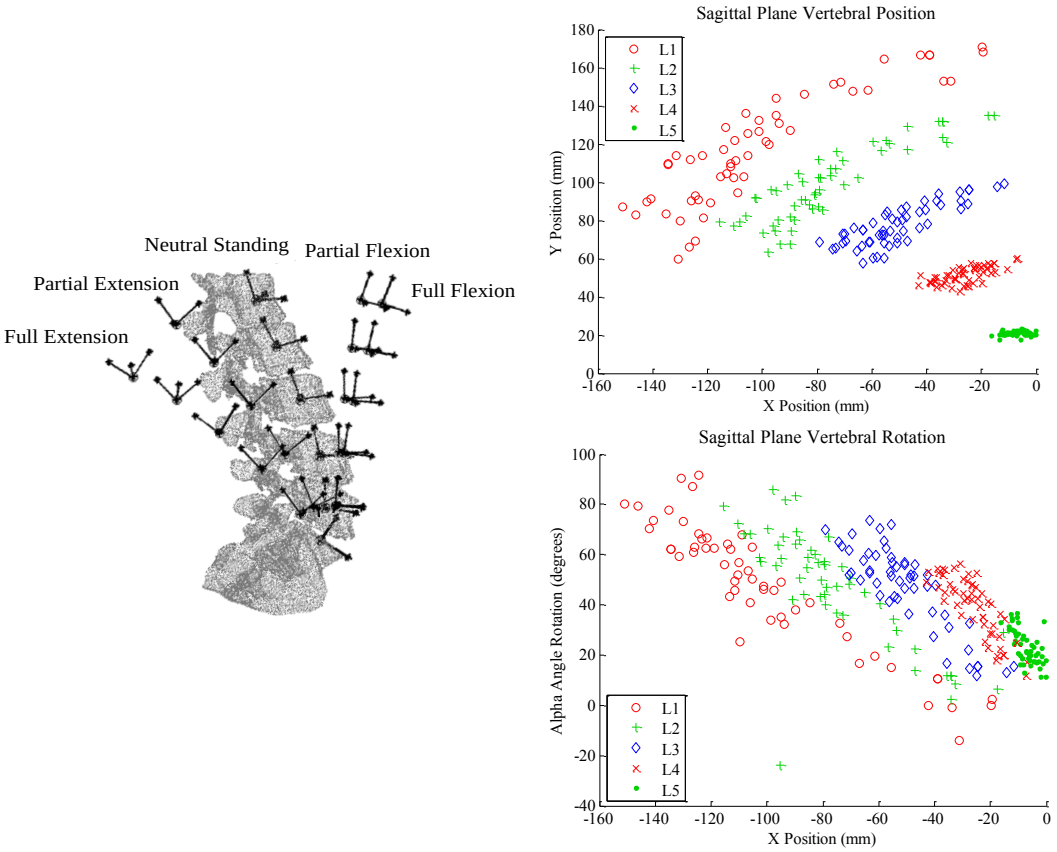

Figure 5.1: Digitized reconstruction of lumbar spine in neutral standing position. Vertebral coordinate systems shown for the range of flexion and extension positions (left). Sagittal plane vertebral position data for 10 subjects performing six flexion-extension postures (top right) and sagittal plane vertebral rotation versus anteroposterior position (bottom right).

Each measurement represents a discrete point on or near the continuum comprising the full range of feasible positions for that vertebra. It is assumed that healthy vertebral motion will be smooth and continuous. A principal component-based approach is implemented to determine the manifold most likely to produce the subset of measured points. Because the measurements presented here are limited to sagittal plane position and rotation, the feasible positions for each vertebra are represented as a one dimensional manifold (a two dimensional planar curve). Vertebral position and angular rotation in the sagittal plane were each modeled using an implicit function (Eq. 1) that consists of anthropometric data (height, weight, age) and measured coordinates with linear and quadratic terms.

$$A_0 + \sum_{i=1}^{m}\sum_{j=1}^{n} A_{ij}\, p_i q_j = 0 \tag{5.1}$$

The vector q contains the geometric constraints for each elliptical manifold. In this case, $q = \{x \quad y \quad x^2 \quad xy \quad y^2\}$ for the manifold that describes planar vertebral position and $q = \{x \quad \alpha \quad x^2 \quad x\alpha \quad \alpha^2\}$ for the manifold that describes the relationship between vertebral rotation, α, and anteroposterior position, x. The vector $p = \{1 \quad h \quad w \quad a\}$ includes terms to evaluate the interaction between vertebral measurements and other measured characteristics such as height, h, weight, w, and age, a. When including these components, each implicit function includes 20 variable terms and a constant, A_0.

The coefficients, A_{ij}, were parameterized using principal component regression. Principal component regression minimizes the perpendicular distance between the implicit function and the measured coordinates through the following five-step process:

Step 1: Measurements from all subjects are grouped according to vertebra and arranged into matrices. The matrices are arranged such that the columns contain the measurement terms and each row contains values from a subject in one of the six positions. The columns are comprised of the linear and quadratic measurement values and the anthropometric interaction terms (contained in vector *p* in equation 1). With the current data set, this results in a 60 x 20 data matrix for each vertebra:

$$\begin{array}{r} \textbf{Row 1}\text{: subject \#1, full extension} \rightarrow \\ \textbf{Rows 2 - 59} \rightarrow \\ \textbf{Row 60}\text{: subject \#10, full flexion} \rightarrow \end{array} \begin{pmatrix} x & y & x^2 & xy & y^2 & \cdots & ax & ay & ax^2 & axy & ay^2 \\ & & & & & \ddots & & & & & \\ x & y & x^2 & xy & y^2 & \cdots & ax & ay & ax^2 & axy & ay^2 \end{pmatrix} \quad (5.2)$$

Step 2: Compute the covariance of each matrix from step 1. This produces a 20 x 20 covariance matrix for each vertebra.

Step 3: Compute the eigenvalues and eigenvectors for each covariance matrix. For each of the five covariance matrices this produces 20 eigenvalues, and each eigenvalue corresponds to a 20 term eigenvector.

Step 4: The manifold coefficients, A_{ij} from equation 1, are parameterized by the eigenvector terms. The first coefficient, A_{11}, is taken from the first eigenvector component and the twentieth coefficient, A_{45}, is taken from the twentieth eigenvector component. The relative magnitude of each coefficient indicates how much the corresponding term influences manifold curvature.

Step 5: The constant term from the implicitly defined manifold, A_0, establishes the manifold centroid and is determined by the eigenvector components and measurement terms as follows:

$$A_0 = -\sum_{i=1}^{20} A_i \overline{m}_i \tag{5.3}$$

where $\overline{m}_i$ is the mean of the i^{th} column of the measurement-data matrix from step 1. That is, $x = \{x, y, x^2, xy, y^2, \ldots, ax, ay, ax^2, axy, ay^2\}$, the set of all measurement terms.

For each vertebra, this process produces 20 eigenvalues (step 3), corresponding to 20 unique manifolds for each set of vertebral measurements. The process does not impose constraints to prevent manifolds without biomechanical relevance, such as hyperbolas. Therefore, the set of manifolds must be evaluated to determine which eigenvalue yields the most accurate, biomechanically feasible manifold. Goodness of fit was evaluated using coefficient of determination, r^2.

5.3 Results

The MR scans produced 60 sets of measurement data per vertebra (10 participants, 6 postures each). Measurements from all participants were grouped according to vertebra and ellipsoid manifolds were determined for describing sagittal plane vertebral position (Fig. 5.2) and rotation (Fig. 5.3). The manifolds include anthropometric effects for subject height, weight, and age. This process produced 20 manifolds for each vertebra. The biomechanically relevant and feasible manifold was identified by visual inspection and goodness of fit. Goodness of fit was assessed with coefficients of determination, r^2, for each vertebra. For sagittal plane vertebral position manifolds, r^2 values ranged from 0.07 for L5 to 0.79 for L1, and for sagittal plane vertebral rotation manifolds, r^2 values ranged from -0.21 for L5 to 0.77 for L1. The biomechanically relevant manifold was not consistently associated with a particular

eigenvalue but it was always found within the range from eigenvalue #2-#7. Coefficient of determination and visual inspection identified the same manifold in every case.

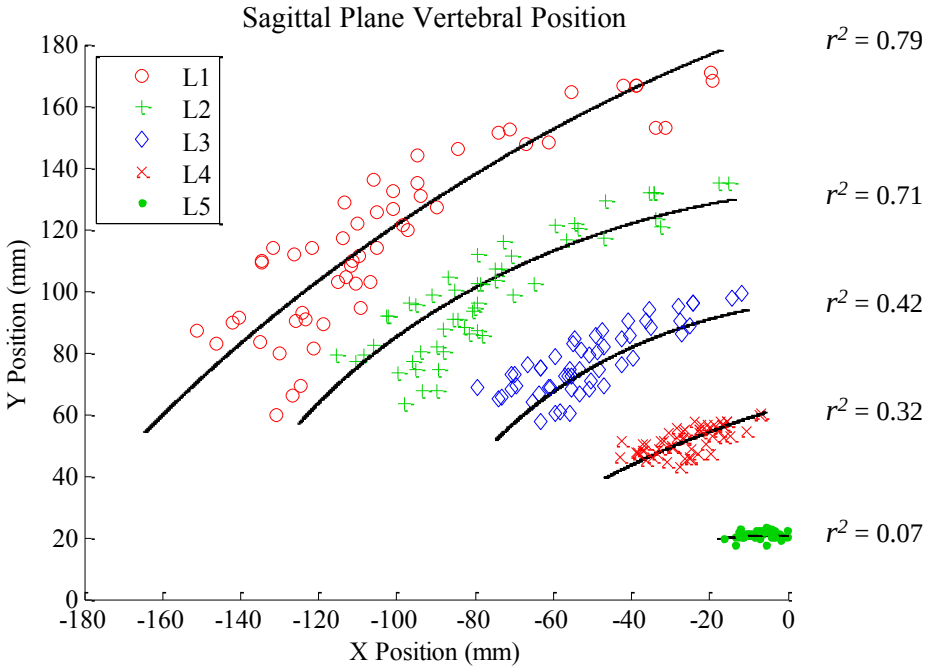

Figure 5.2: Principal component manifolds for sagittal plane position of each lumbar vertebra. Goodness of fit was evaluated using coefficient of determination, r^2.

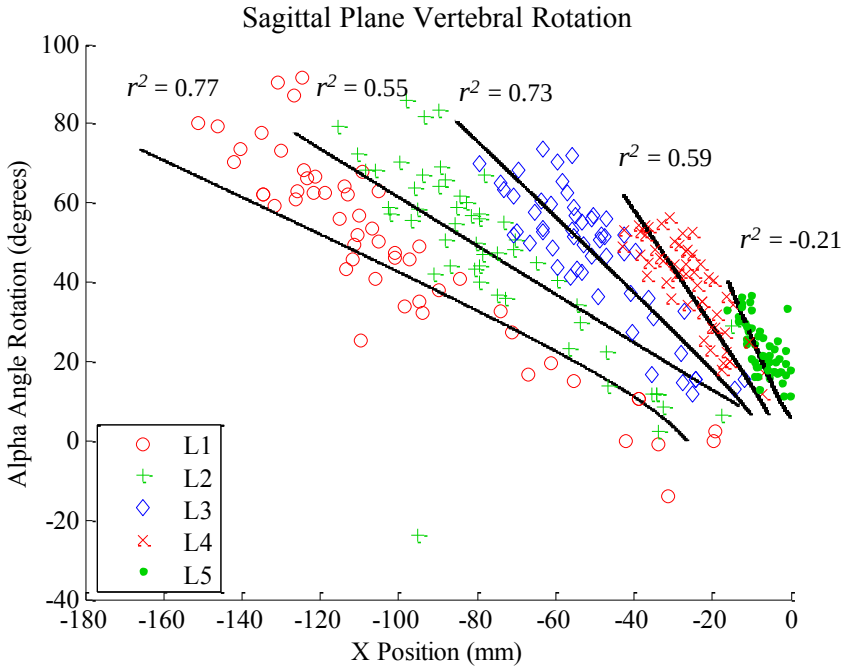

Figure 5.3: Principal component manifolds for sagittal plane vertebral rotation. Goodness of fit was evaluated using coefficient of determination, r^2.

5.4 Discussion

Modeling these positions using geometric manifolds parameterized with principal component regression provides a novel approach for evaluating intervertebral joint configuration. This approach assumes that lumbar vertebral joint trajectory can be modeled using a family of five ellipsoidal manifolds. Low dimensional geometric manifolds are appropriate for this model because the anatomic constraints dictate that healthy vertebral motion should be smooth and continuous. Each of the measured data points is assumed to exist on or near the representative manifold. Principal component regression determines the relationship between the discrete measurements and the continuous manifold that contains them. This procedure uses physiologically-based constraints with minimal computational complexity and includes participant-specific anthropometry to determine parameterized vertebral position along five unique degrees of freedom for sagittal plane vertebral position and five unique degrees of freedom for sagittal plane vertebral rotation during flexion and extension.

When unconstrained, the five lumbar vertebrae have 15 degrees of freedom in the sagittal plane. Musculoskeletal models apply constraints to reduce this to as few as a single degree of freedom (Christophy et al. 2012). Often these are mechanical constraints formulated on standard connections which do not account for the natural vertebral paths, and may not represent key stabilizing features of the lumbar spine such as lumbar lordosis. For models created with a mechanistic foundation, these simplifications are necessary to maintain tractable complexity and the ability to evaluate and interpret the response variable of interest (Wagner et al. 2012). However, these constraints also limit

model applicability, and may hinder validation by preventing comparisons between dissimilar models.

By comparison, principal component regression makes minimal assumptions about the mechanism responsible for kinematics but can describe complex joint motion by incorporating ellipsoidal geometry and inferring a mechanistic outcome through the relationship between all available input data (comprised of subject specific vertebral measurements and anthropometry). Previous geometric models have used regression techniques that lack kinematics-based constraints and have required complex, sequential transformation and regression steps (Sicard & Gagnon 1993), increasing computational load and potential for error propagation. Principal component regression provides a modular structure that can be expanded with nominal added complexity to evaluate any contributing factor of interest.

Principal component regression created 20 parameterized manifolds for each vertebra. Therefore, the curves must be evaluated to determine which one most accurately represents the intervertebral kinematics that provided the measured data. Curves were evaluated for goodness of fit using coefficient of determination, r^2. While r^2 is convenient and successfully identified the curve corresponding to the best visual fit, it is not a fully appropriate metric for evaluating goodness of fit for implicit function regression. Coefficient of determination evaluates fit by treating y as the dependent variable. Implicit function regression parameterizes manifolds by minimizing orthogonal distance to all points. This approach assumes that measurement error is equally likely in any rectangular direction, which reflects reality. Consequently, the biomechanically relevant manifold will pass through the "middle" of a data cloud comprised of vertebral measurements and

will be a directed along the path of greatest variance. Of course, only one curve can achieve this for a given set of points. The remaining curves represent some other characteristic of the data, such as measurement error, in accordance with its variance. The specific eigenvalue (1^{st}, 2^{nd}, 3^{rd}, etc.) that correctly describes the kinematic manifolds depends on the variance within the true data and the relative magnitude and distribution of measurement error (Fig. 5.4).

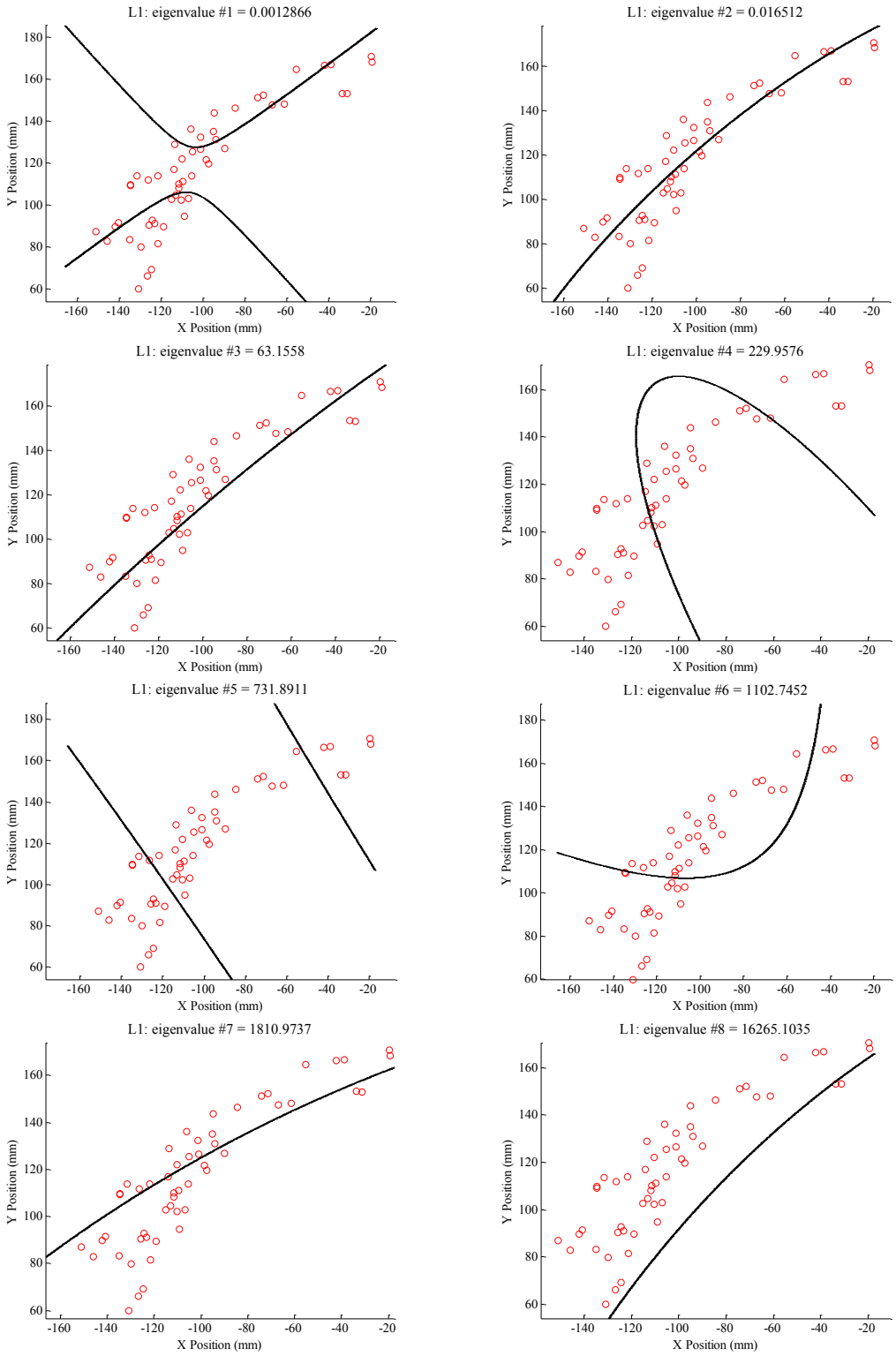

Figure 5.4: Principal component manifolds for the first eight eigenvalues with L1 sagittal plane measurement data. Eigenvalue #2 (top right) appears to provide the best kinematic description and has the highest coefficient of determination, r^2, = 0.79. Curves are similar for all vertebrae.

In addition, r^2 values are of not necessarily beneficial for determining a poor fit. This is because values are dependent upon data sample size, range, and distribution (Cornell & Berger 1987). For example, the curves for L5 presented in Figures 5.2-3 have relatively low r^2 values despite a good visual fit.

When the kinematic manifolds are created using a statistically representative data set, the model should be able to make accurate, subject-specific predictions. Because the model structure is not limited by mechanical simplifications, we expect that it will be capable of subject -specific predictions with low generalization error. Prior to making subject-specific predictions, an evaluation of terms will be performed to ensure that the model is optimized to achieve maximum accuracy with minimal complexity. This evaluation will be performed though an information criterion and model terms that do not improve accuracy will be removed. Conversely, to improve accuracy, the implicit function may require additional anthropometric terms that have not yet been considered. For example, visual inspection of the results indicates that there is greater variance in extension positions than flexion. Visual evaluation of anthropometric trends within the measured points may provide insight into anthropometric factors that can improve model accuracy (Figure 5.5). From the anthropometry presented, both gender and height indicate some visual correlation with vertebral position in extension postures.

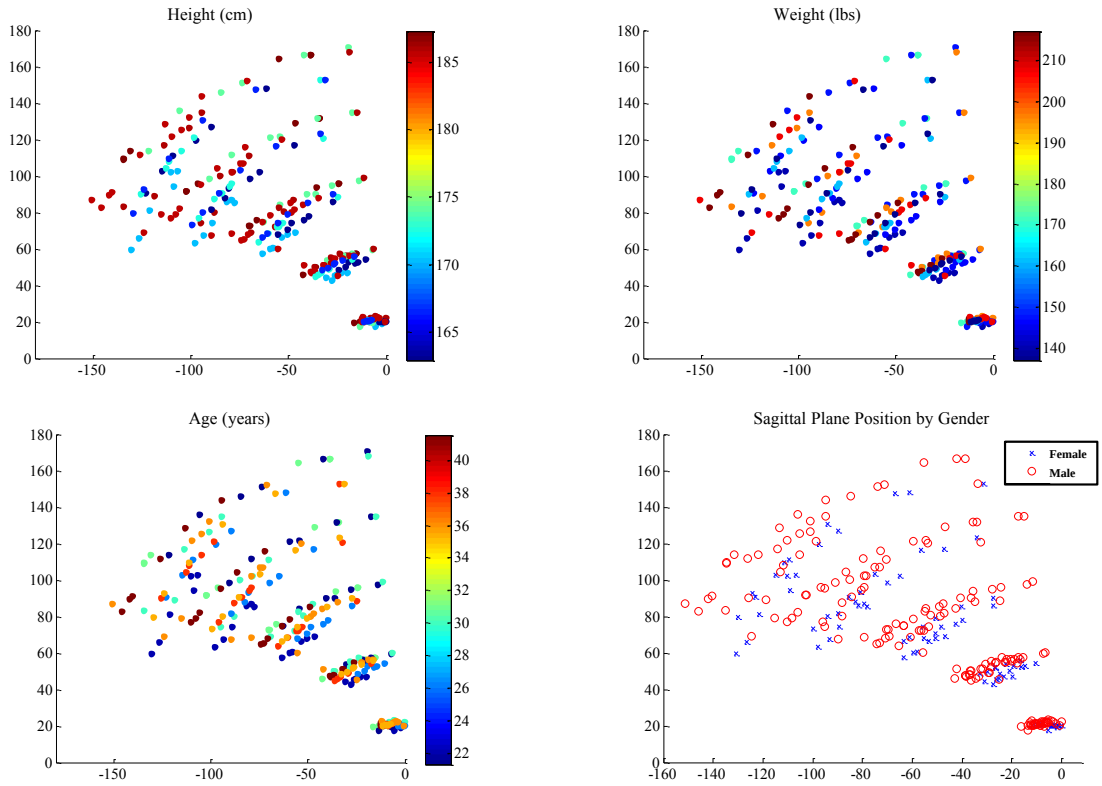

Figure 5.5: Sagittal plane measurements plotted with anthropometric data. Subject height and gender indicate visual correlation with vertebral position during extension postures.

5.5 Conclusion

Principal component-based modeling offers unique advantages for predicting and interpreting performance of complex systems such as lumbar joint biomechanics because no assumptions are made regarding the governing mechanisms. This provides an opportunity to infer mechanistic characteristics about intervertebral joint kinematics and to use *in vivo* data to validate musculoskeletal models. However, this intentionally general and minimally constrained model structure allows for biomechanically infeasible manifolds are a subset of the solution space. Therefore, it is important to evaluate the solutions for biomechanical relevance and interpretability when using this method.

6. Intervertebral joint kinematics of the lumbar spine

6.1 Introduction

Investigating intervertebral joint kinematics of the lumbar spine could improve understanding of healthy and pathological joint mechanics and the associated tissue loading. This information is valuable for identifying root causes of pathological conditions and could thereby influence preventative actions and rehabilitation treatments as well as establish standards for motion preserving arthroscopic implant design.

Configuration of the full lumbar spine represents the combined contributions from the individual intervertebral lumbar joints. Five intervertebral joints spanning the lumbar spine from L1 to the sacrum are comprised of two adjacent vertebrae separated by a viscoelastic intervertebral disc (IVD). Each intervertebral joint forms a functional spinal unit (FSU) capable of three translational and three rotational degrees of freedom.

Joint configuration influences the tissue loading on the articular surfaces and the intervertebral discs. Vertebral displacement from a neutral joint position causes intervertebral disc deformation and may induce contact forces at the articular surfaces of the facet joints. Load distribution and magnitudes experienced within the IVD and at the articular surfaces varies with the specific joint configuration as well as with the applied external loads from adjacent musculoskeletal structures. Understanding these loadings

can provide insight into degenerative pathological conditions in the lumbar spine. I*n vivo* measurement data can be used to develop, refine, and validate musculoskeletal models of lumbar intervertebral joint kinematics.

Musculoskeletal models have been developed to evaluate loading on the lumbar spine (Marras & Granata 1997; Aspden 1988). However, without accounting for specific intervertebral joint orientation, these models cannot determine the shear and compressive tissue loads, which limits their usefulness for understanding failure modes and injury mechanisms. Recently, at least one model addressed this limitation by including lumbar FSU configuration in several standing flexion postures (Splittstoesser et al. 2011) but the evaluation is limited to sagittal plane rotation between vertebrae.

Dunk et al. (2009) demonstrated clinical relevance of lumbar intervertebral joint kinematics related to understanding the mechanisms for pathological tissue loading. The study used sagittal planar radiographs to evaluate intervertebral angle at each FSU between L3 and the sacrum in a series of standing and seated postures with different degrees of flexion. The results indicated that seated postures induce substantial lumbar flexion at the inferior vertebral joints compared with neutral standing postures. The increased tissue loads associated with lumbar flexion lead to increased susceptibility to soft tissue damage at the flexed joint. Tissue stress related to prolonged seated postures may be one mechanism for soft tissue damage.

Understanding FSU kinematics is particularly useful for guiding development of orthopedic vertebral disc replacements that aim to preserve natural kinematic performance (Zander et al. 2009; Galbusera et al. 2008). Artificial disc replacement surgery is performed to treat degenerative intervertebral disc conditions. The ability to

preserve natural kinematic performance within an artificial disc is believed to benefit the adjacent FSUs. By comparison with artificial disc replacements that preserve vertebral kinematics, spinal fusion procedures are believed to create kinematic overcompensation and overload in adjacent vertebral joints, leading to accelerated disc degradation within those FSUs (Stokes & Iatridis 2004).

In vivo data of FSU kinematics measured across the range of joint motion may also help elucidate poorly understood vertebral mechanics including coupled vertebral joint motion and secondary rotations (Legaspi & Edmond 2007). There is a lack of consensus regarding precisely what types of coupled intervertebral motion patterns occur and what causes them. There is also a lack of understanding regarding the motion sequences for multi-joint intervertebral motions. Gatton and Pearcy (1999) observed that individuals performing specific lumbar motions initiate vertebral movement using different joint motion sequences. Current models do not account for these differences.

The objective of this investigation is to investigate the ability to evaluate six degree-of-freedom intervertebral lumbar joint kinematics *in vivo* through a range of joint motion under normal loading conditions.

6.2 Methods

Positional magnetic resonance imaging (MRI) data was collected from two healthy participants with no history of low back pain or injury (SUBJECT ‘A’: male, 41 years; SUBJECT ‘B’: female, 35 years) using a FONAR 0.6-Tesla Upright scanner. Scans were captured in six standing flexion and extension postures (full extension, partial extension, neutral standing, 1/3 flexion, 2/3 flexion, full flexion). Digitized three-dimensional reconstructions of the lumbar vertebrae and sacrum were created for each

MR scan and body-fixed coordinate systems were assigned to each vertebra and sacrum. The process for creating digitized three-dimensional reconstructions and coordinate system assignment convention was consistent with the details provided in chapter 3. The coordinate systems provided measurements for rectangular position (x,y,z) and angular rotation (α,β,γ) of each FSU in each posture. FSU measurements were recorded as the position and angular rotation of the superior vertebral coordinate system relative to the inferior vertebral coordinate system. Measurements were recorded for each FSU spanning from L1 to the sacrum (L1-L2, L2-L3, L3-L4, L4-L5, and L5-S1). Angular rotation of the superior FSU vertebra was measured using Cardan angles and the first rotation, α, was about the lateral axis (z-axis), indicating vertebral rotation in the sagittal plane (Figure 6.1). The second and third Cardan angles (β and γ, respectively) provide angular rotation about the successively rotated A-P (x) and S-I (y) vertebral axes.

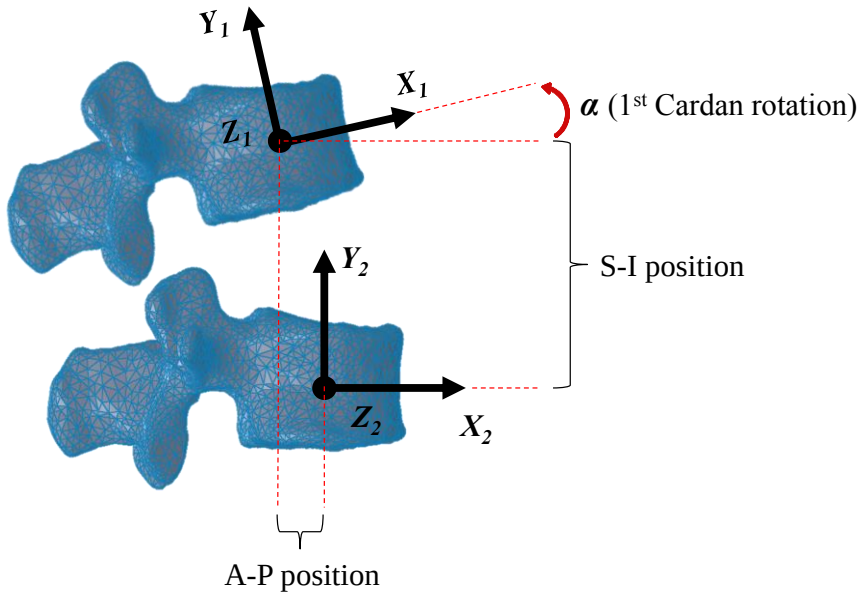

Figure 6.1: Schematic diagram of FSU measurement convention (side view). Reported measurements indicate rectangular position (x, y, z) and Cardan rotation of the superior vertebral coordinate system relative to the inferior vertebral coordinate system. Note that lordosis results in negative A-P position values and positive α angle values.

6.3 Results

Measurement results are presented for all six dependent variables (rectangular position (x,y,z) and angular rotation (α,β,γ)) for both study participants. For each dependent variable, results are presented twice. First, to evaluate individual joint kinematics across the range of motion, measurements are presented for each FSU in all six flexion-extension postures. Second, for each posture the results are presented for every FSU to demonstrate the individual contributions of each joint to specific posture.

To facilitate comparisons between individuals, results for each dependent variable are presented first for Subject ‘A’ and then for Subject ‘B’. Results are presented first for rectangular position measurements followed by angular rotation measurements.

Superior-inferior position measurements for Subject 'A':

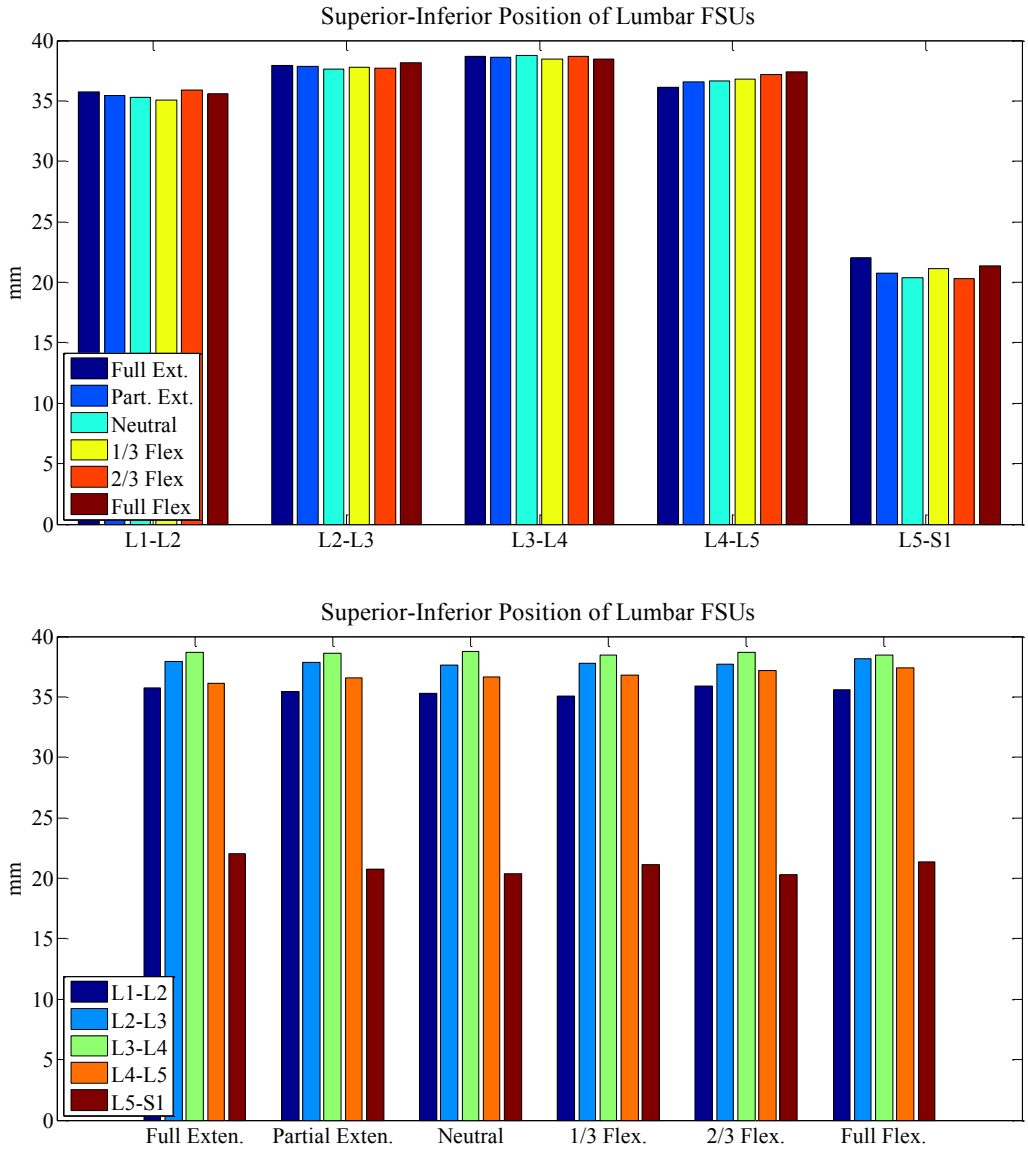

Figure 6.2: SUBJECT 'A': Superior-inferior FSU measurements during six standing flexion-extension postures. Results presented for individual joints across the full range of postures (top) and for all joints at a given posture (bottom).

Superior-inferior position measurements indicate less displacement in the L5-S1 joints than in the superior joints. Total displacement across the range of postures is small (< 5mm) for each joint. L4-L5 demonstrates a modest amount of traction when moving

from extension to flexion. The greatest S-I magnitude is observed in L3-L4 for all postures.

Superior-inferior position measurements for Subject 'B':

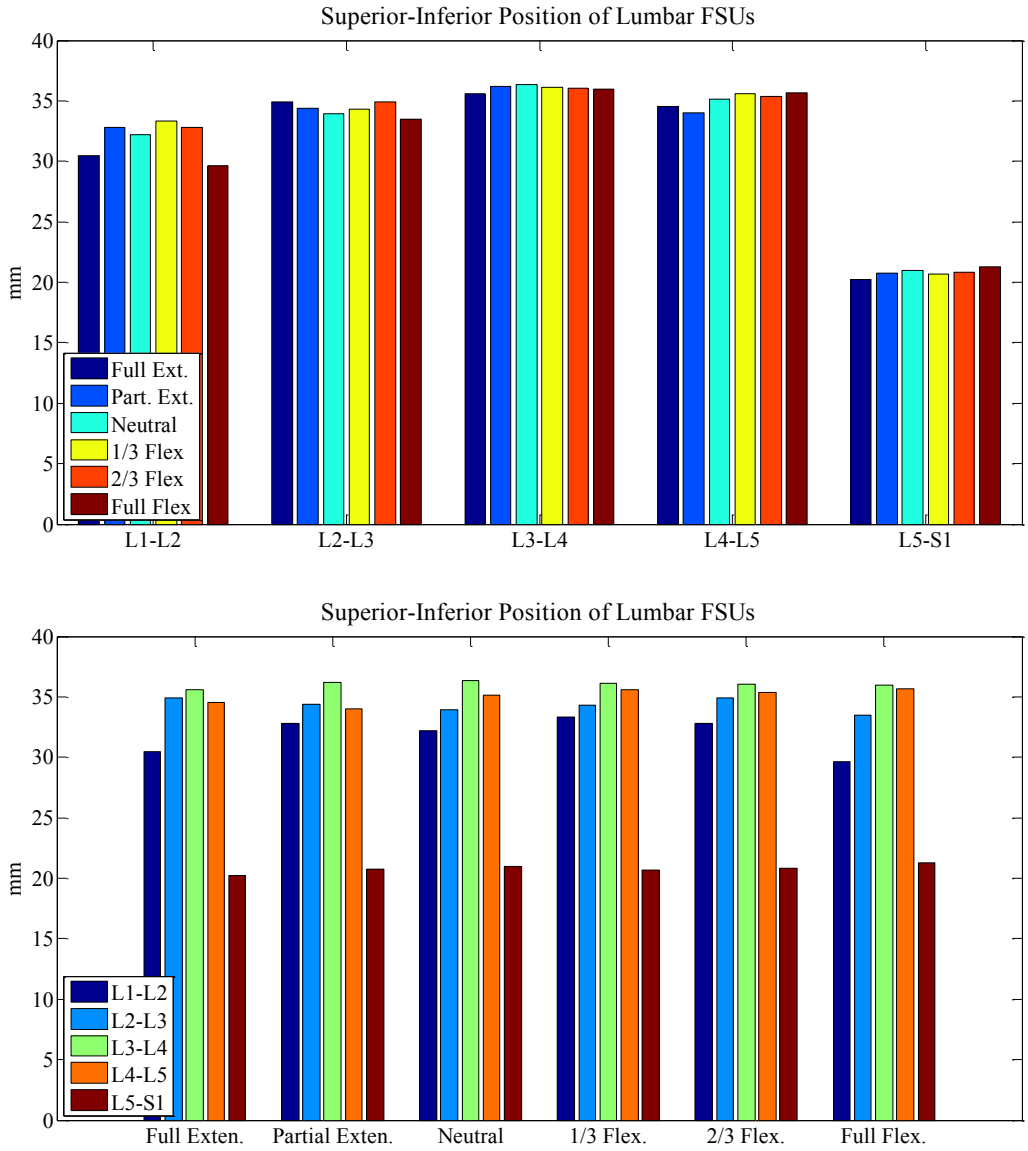

Figure 6.3: SUBJECT 'B': Superior-inferior FSU measurements during six standing flexion-extension postures. Results presented for individual joints across the full range of postures (top) and for all joints at a given posture (bottom).

Subject 'B' demonstrates the same characteristics noted for Subject 'A'. By comparison with the other dependent variables, S-I measurements demonstrated the greatest overall consistency between subjects.

Anterior-posterior position measurements for Subject 'A':

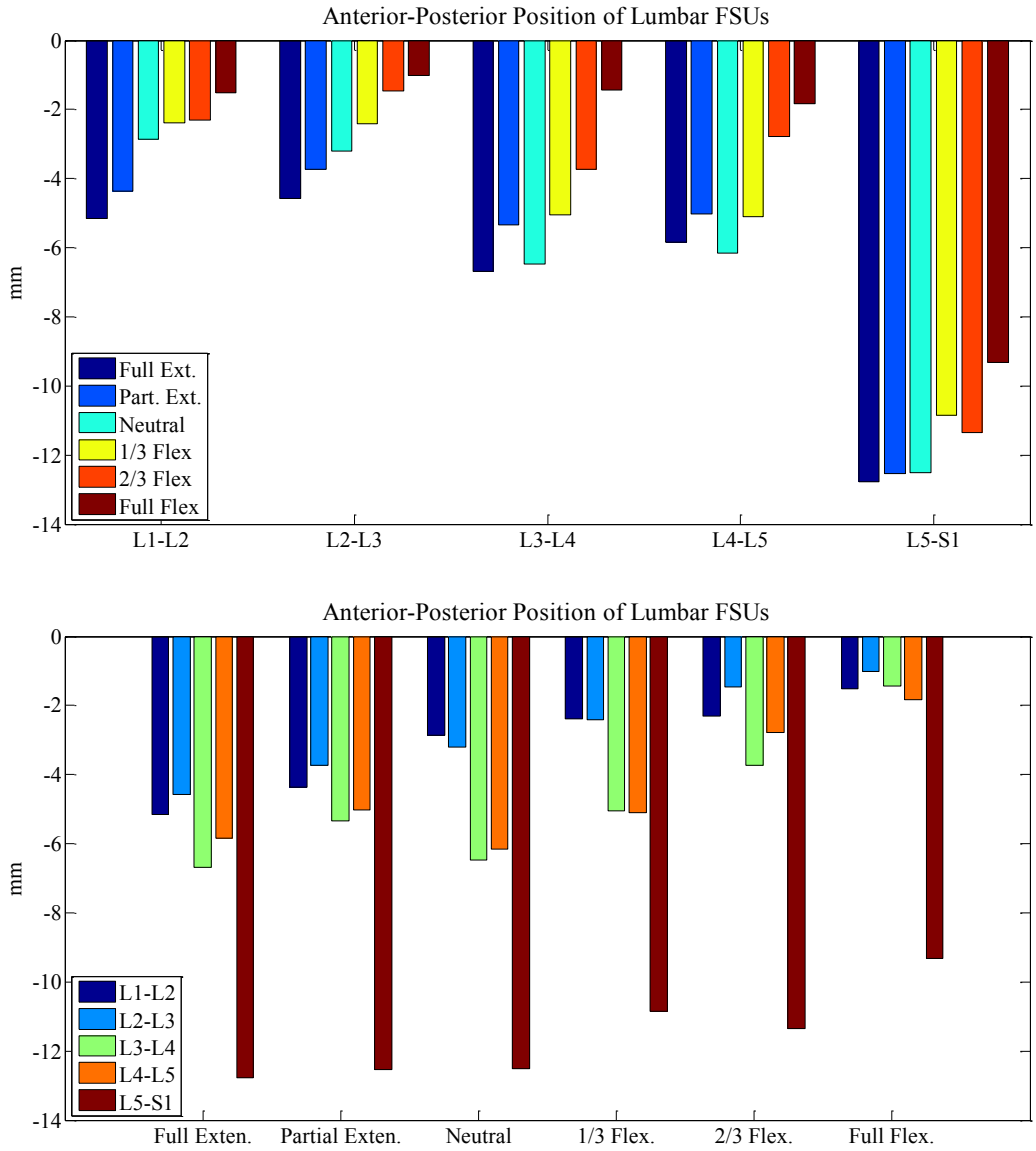

Figure 6.4: SUBJECT 'A': Anterior-Posterior FSU measurements during six standing flexion-extension postures. Results presented for individual joints across the full range of postures (top) and for all joints at a given posture (bottom).

Lordosis dictates that the superior vertebra will be located posterior to the inferior vertebra, producing a negative value for anterior-posterior position. The superior vertebra moves anteriorly during flexion, producing profressively less-negative measurement values at each joint. This trend is most noticeable at the L1-L2 and L2-L3 joints, where

the trend produces an approximately linear increase in A-P position. Posterior displacement is greatest in the L5-S1 joint.

Anterior-posterior position measurements for Subject 'B':

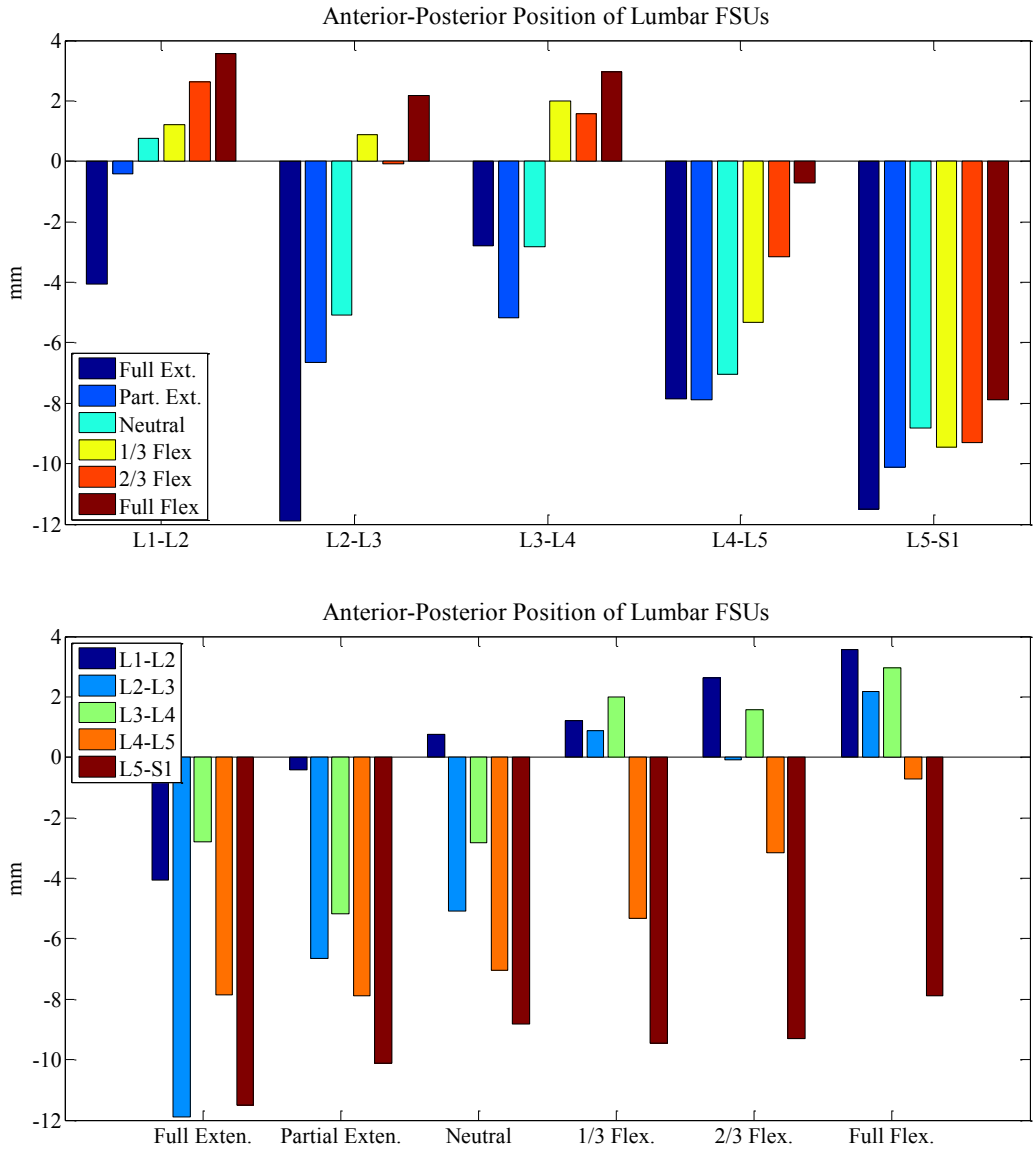

Figure 6.5: SUBJECT 'B': Anterior-Posterior FSU measurements during six standing flexion-extension postures. Results presented for individual joints across the full range of postures (top) and for all joints at a given posture (bottom).

Characteristics noted for Subject 'A' also apply to Subject 'B'. However, whereas A-P position remained negative across all postures for Subject 'A', Subject 'B' demonstrates anterior displacement of the superior vertebra at L1-L2, L2-L3, and L3-L4 during flexion, resulting in positive measurement values.

Medial-lateral position measurements for Subject 'A':

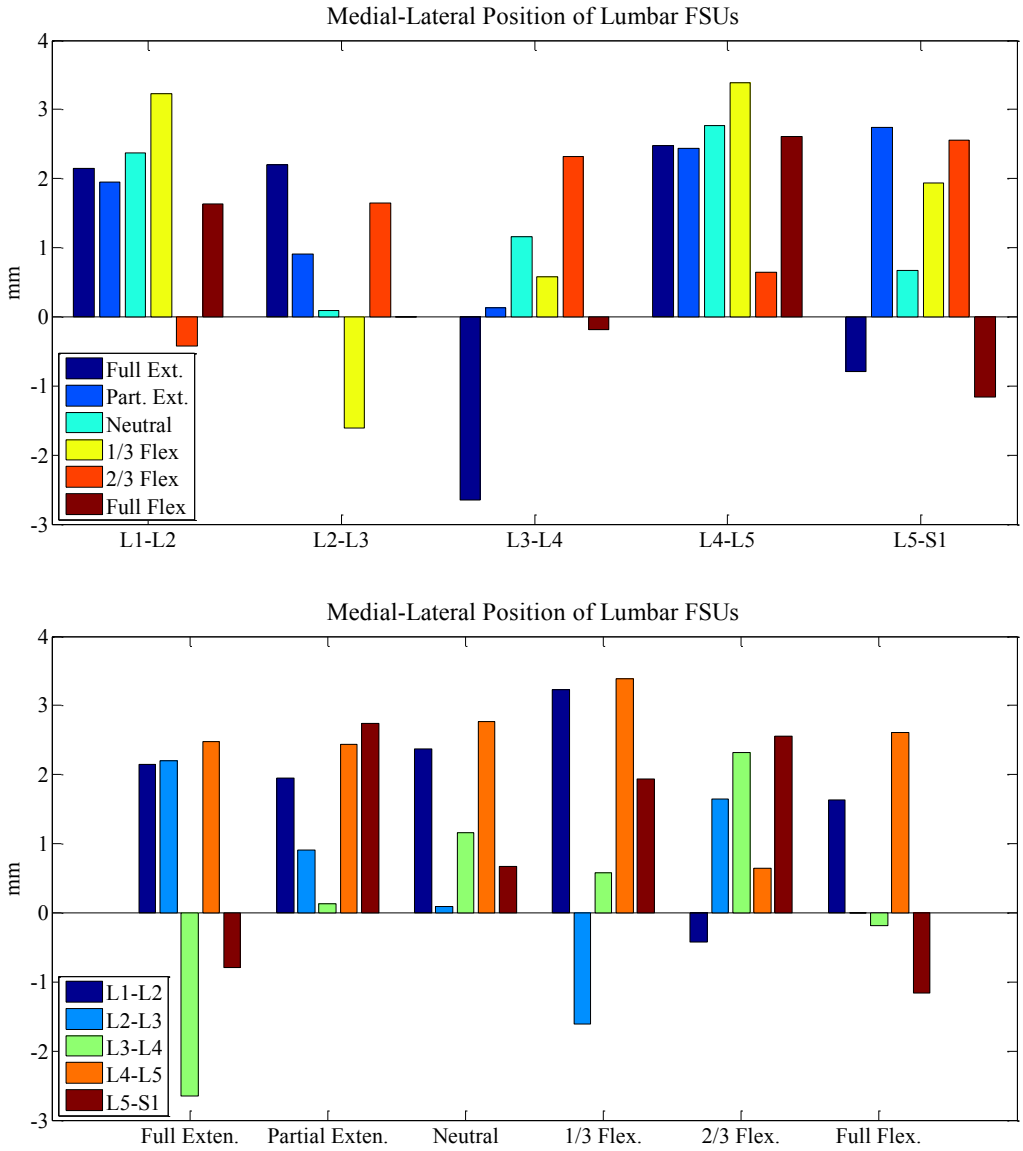

Figure 6.6: SUBJECT 'A': Medial-Lateral FSU measurements during six standing flexion-extension postures. Results presented for individual joints across the full range of postures (top) and for all joints at a given posture (bottom).

During sagittal plane dominated movements such as flexion-extension, medial-lateral displacements have lower magnitude and trends are less obvious. However, M-L displacements appear to be correlated between L1-L2 and L4-L5. Positive measurement

values indicate that the superior vertebra is displaced laterally to the right of the inferior vertebra. All M-L displacements are relatively small (< 3mm).

Medial-lateral position measurements for Subject 'B':

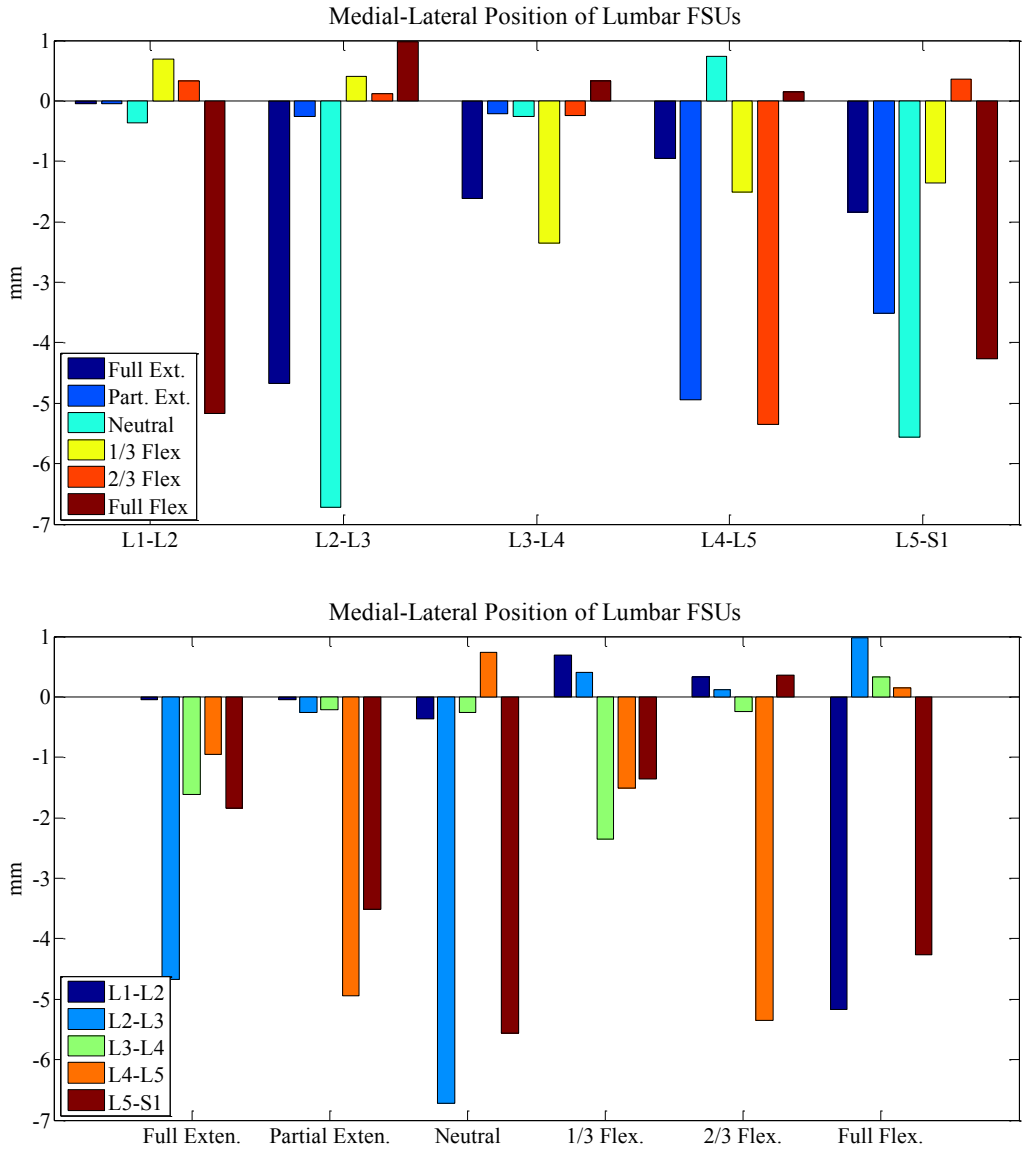

Figure 6.7: SUBJECT 'B': Medial-Lateral FSU measurements during six standing flexion-extension postures. Results presented for individual joints across the full range of postures (top) and for all joints at a given posture (bottom).

No clear M-L displacement trends are visible for Subject 'B'. Unlike Subject 'A', the measurement values are primarily negative, indicating that the superior vertebra is displaced laterally to the left of the inferior vertebra.

Sagittal plane rotation measurements for Subject 'A':

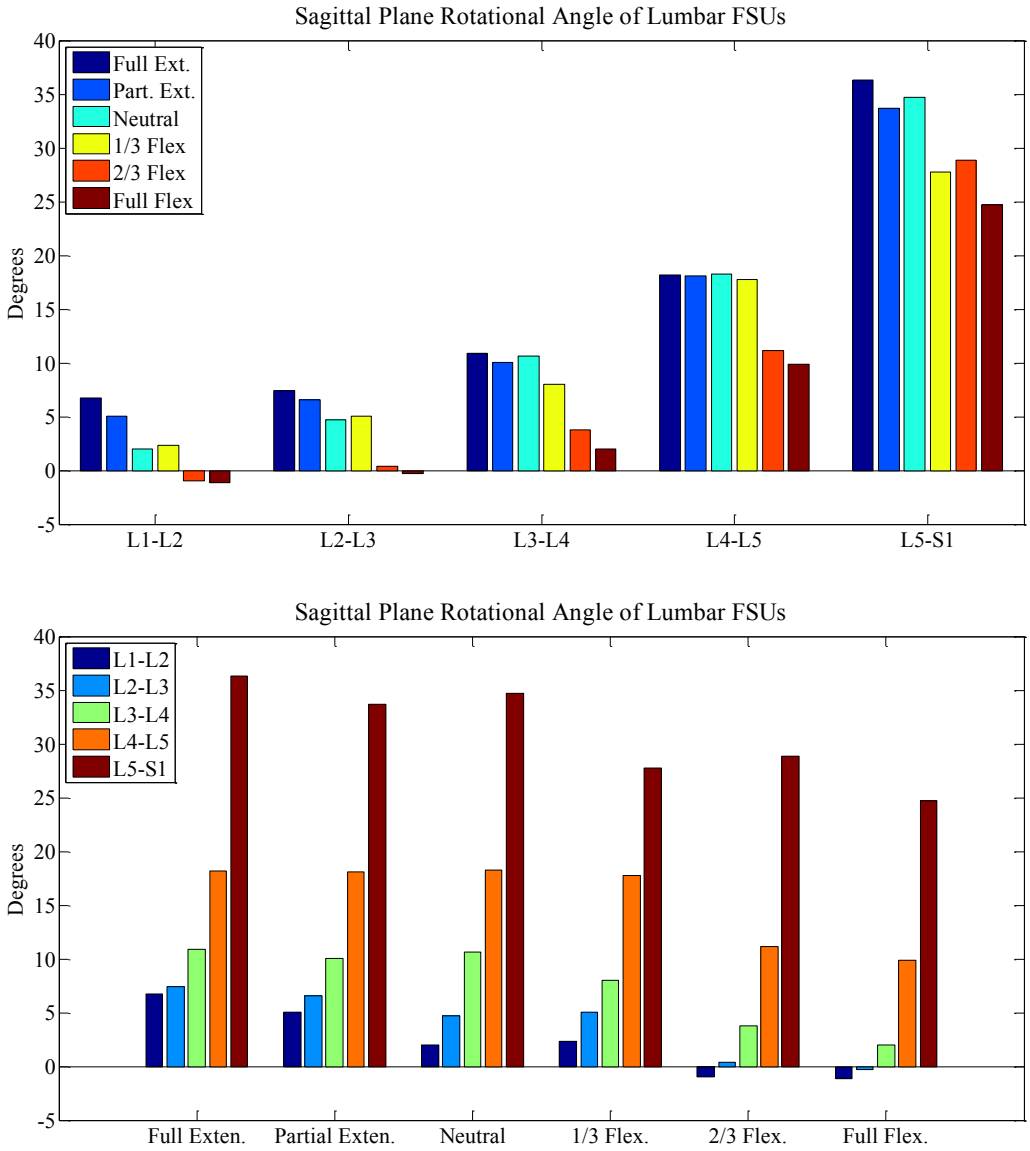

Figure 6.8: SUBJECT 'A': Sagittal plane rotation (1st Cardan angle, α) FSU measurements during six standing flexion-extension postures. Results presented for individual joints across the full range of postures (top) and for all joints at a given posture (bottom).

A positive α-angle indicates that the superior vertebra is rotated posteriorly about the M-L axis relative to the inferior vertebra, as would be expected in lordosis. Inferior joints demonstrate greater rotational magnitudes than the superior joints. In addition, the inferior joints demonstrate a greater rotational range of motion than the superior joints.

Specifically, L5-S1 rotates 12° between full extension (37°) and full flexion (25°) whereas L1-L2 rotates 8° (7° in full extension to -1° in full flexion).

Sagittal plane rotation measurements for Subject 'B':

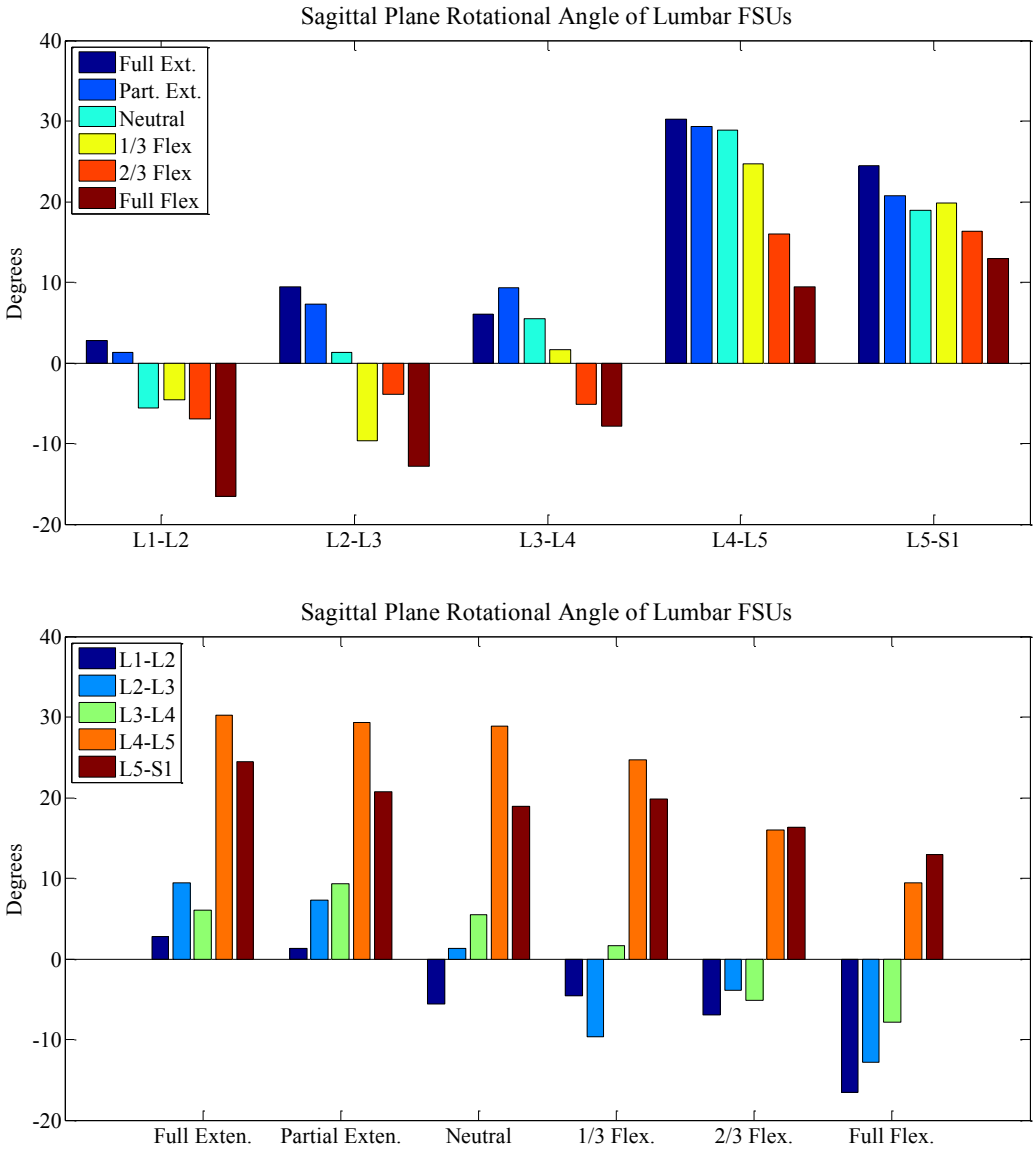

Figure 6.9: SUBJECT 'B': Sagittal plane rotation (1st Cardan angle, α) FSU measurements during six standing flexion-extension postures. Results presented for individual joints across the full range of postures (top) and for all joints at a given posture (bottom).

Subject 'B' demonstrates similar α-angle characteristics as Subject 'A'. However, the magnitude is smaller at each joint level and for each position, indicating less lordotic curvature. This is consistent with the A-P measurements for Subject 'B', which demonstrated more anterior displacement, indicating less lordotic curvature.

Unlike Subject ‘A’, α-angle magnitude and range of motion are greatest at L4-L5 (spanning from 30° to 10°) and decrease slightly at L5-S1 (spanning from 25° to 15°).

2nd Cardan angle rotation measurements for Subject 'A':

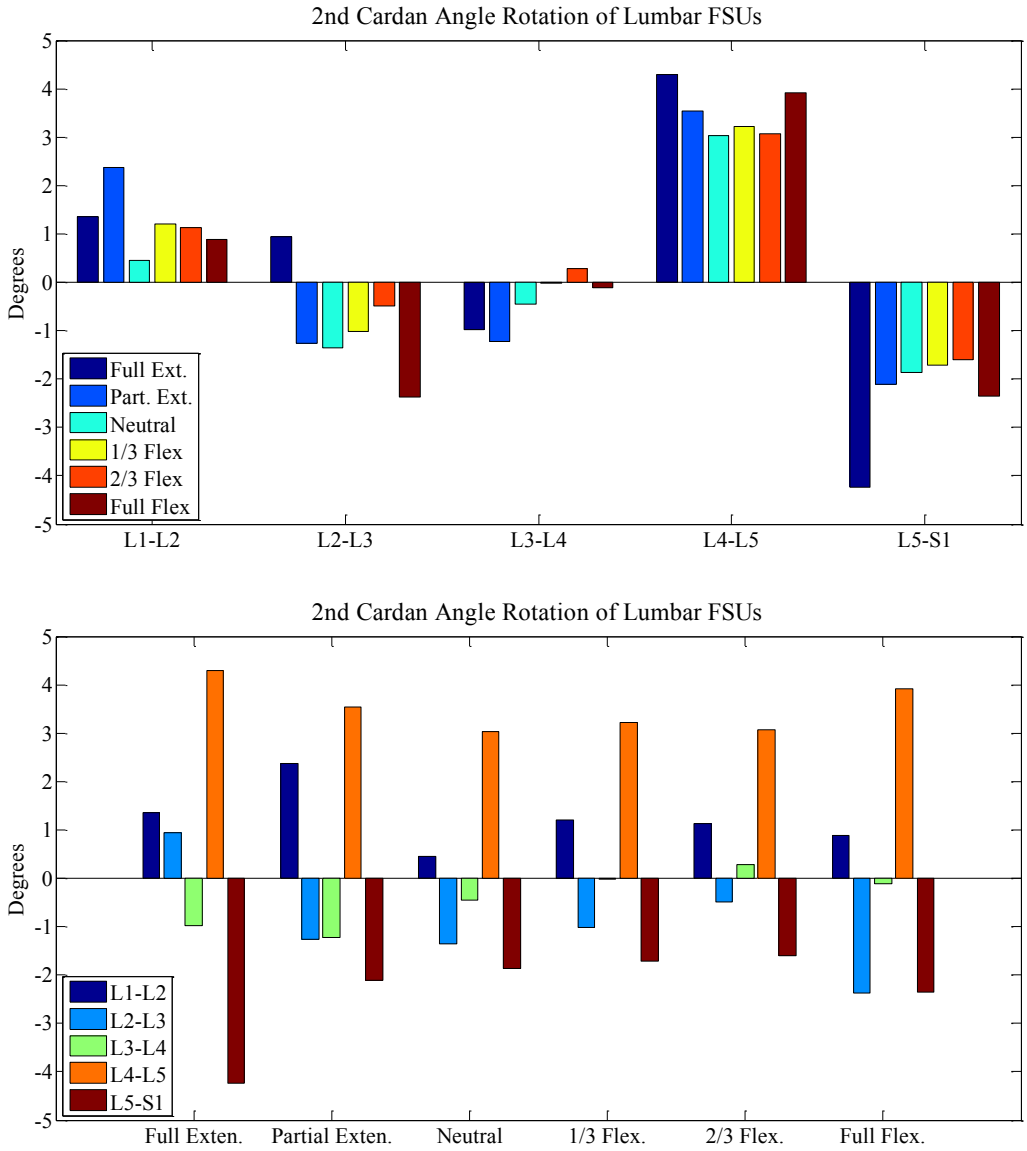

Figure 6.10: SUBJECT 'A': 2nd Cardan angle (β) (rotation about the α–rotated A-P axis) FSU measurements during six standing flexion-extension postures. Results presented for individual joints across the full range of postures (top) and for all joints at a given posture (bottom).

The 2nd Cardan angle (β) provides rotation measurement about the rotated A-P axis of the superior vertebra, roughly corresponding to a lateral bend. Positive values indicate curvature towards the right lateral side. Like the M-L displacement measurements, β-angle trends are less obvious than sagittal plane variables for the

flexion-extension postures being studied. The most noticeable trend is a negative correlation between adjacent FSUs at L4-L5, L5-S1 and at L1-L2, L2-L3. This may indicate coupled counter rotations about the A-P axes in adjacent joints.

2nd Cardan angle rotation measurements for Subject 'B':

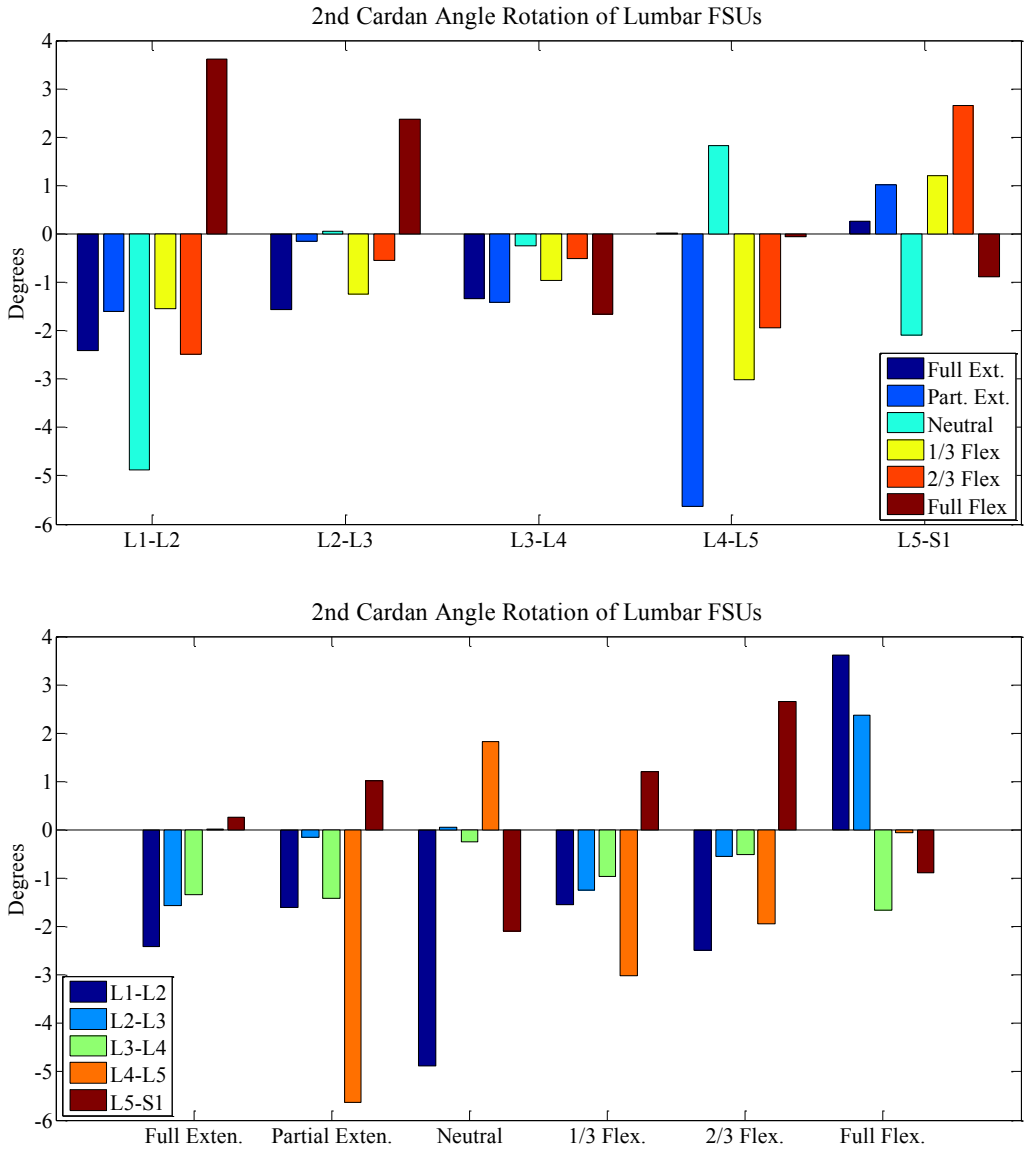

Figure 6.11: SUBJECT 'B': 2nd Cardan angle (β) (rotation about the α–rotated A-P axis) FSU measurements during six standing flexion-extension postures. Results presented for individual joints across the full range of postures (top) and for all joints at a given posture (bottom).

No clear trends are visible for β-rotation measurements in Subject 'B'. There appears to be a modest trend from negative rotational measurements to positive rotational measurements as postures move from extension to flexion.

3rd Cardan angle rotation measurements for Subject 'A':

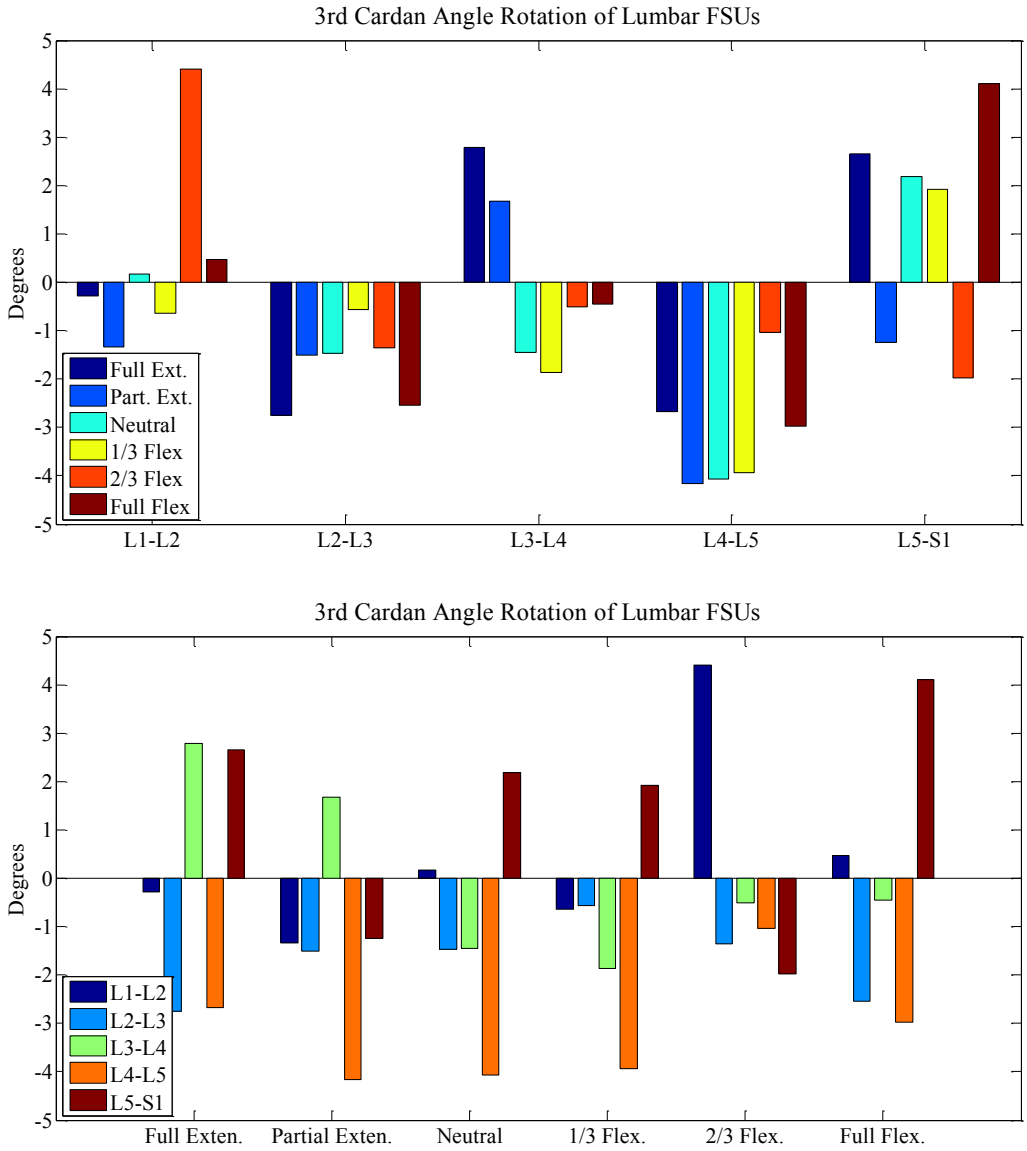

Figure 6.12: SUBJECT 'A': 3rd Cardan angle (γ) (rotation about the β–rotated S-I axis) FSU measurements during six standing flexion-extension postures. Results presented for individual joints across the full range of postures (top) and for all joints at a given posture (bottom).

The 3rd Cardan angle (γ) provides rotation measurement about the β–rotated S-I axis, roughly corresponding to an axial rotation. There are no obvious visible trends although there may be a negative correlation between adjacent joints based on the

alternately negative and positive (or less-negative) values observed at adjacent joints. This may indicate coupled counter rotations about the S-I axes in adjacent joints.

3rd Cardan angle rotation measurements for Subject 'B':

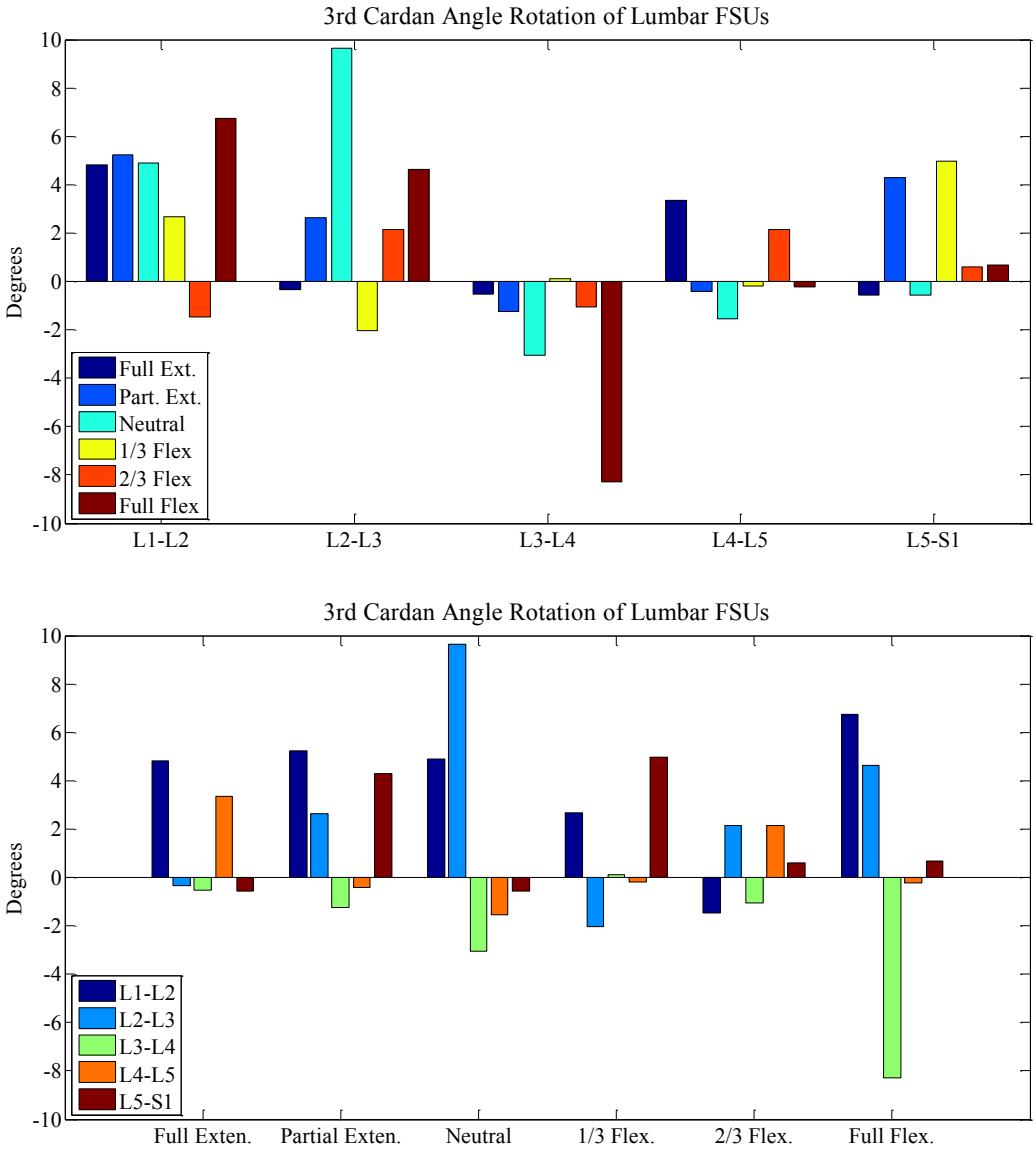

Figure 6.13: SUBJECT 'B': 3rd Cardan angle (γ) (rotation about the β–rotated S-I axis) FSU measurements during six standing flexion-extension postures. Results presented for individual joints across the full range of postures (top) and for all joints at a given posture (bottom).

No clear trends are visible for γ-rotation measurements in Subject 'B'.

6.4 Discussion

Measurement results presented here describe six degree of freedom joint position across six standing flexion-extension postures performed under normal gravitational loading conditions. Because the intervertebral lumbar joints form the constituent components of the lumbar spine, intervertebral joint kinematics provide insight into full lumbar spine kinematics in addition to single joint kinematics. Based on data from two healthy subjects, flexion-extension lumbar kinematics are primarily described by intervertebral anterior-posterior translation and sagittal plane rotation. By comparison, superior-inferior translational position does not vary as greatly across the range of postures. The three non-sagittal plane measurements (M-L position, and 2^{nd} and 3^{rd} Cardan angles) either demonstrate low variation (Figure 6.8) or are characterized by irregular variation that suggests possible measurement error (Figure 6.7).

Results indicate the greatest rotational joint mobility occurs at the inferior lumbar joint segments. Sagittal plane rotational mobility, calculated as the difference between the 1^{st} Cardan angle (α) in full extension and full flexion, was greatest at L5-S1 for the male subject (Subject 'A') (Figure 6.6). In the female subject (Subject 'B') sagittal plane rotational mobility was greatest at L4-L5 with only slightly less mobility measured at L5-S1. By comparison, Dunk et al. (2009) measured sagittal plane rotational mobility for L3-L4, L4-L5, and L5-S1 joints between neutral standing and fully flexed standing positions. Based on data collected from 13 males, Dunk also observed the greatest rotational mobility at the L5-S1 joint. In addition, for 14 female participants, Dunk reported greatest rotational mobility at L4-L5 with slightly less mobility at L5-S1. Comparisons with Dunk are limited to sagittal plane rotation measurements and to joints spanning L3

to the sacrum. Also, Dunk only examined vertebral rotation between neutral standing and forward flexion. Lumbar extension was not considered.

The lumbar spine acts as a kinematic chain originating at the sacrum. Joint mobility propagates superiorly through the lumbar spine such that superior joints reflect the cumulative joint displacements of all inferior joints. This effect produces progressively greater global vertebral displacements at superior vertebrae. When considering subject specific variability for joint mobility in the context of the lumbar spine kinematic chain, this relationship may help explain the relatively broad data dispersion visible within the superior vertebrae in the grouped kinematic measurements in Figure 5.2.

The MR imaging protocol used for data collection was designed to maximize sagittal plane measurement resolution at the expense of lateral measurement resolution. As a result, non-sagittal plane measurements are more susceptible to measurement error, as discussed in Chapter 3. Therefore, sporadic and variable measurement results for medial-lateral position must be interpreted carefully. It is difficult to imagine that the medial-lateral vertebral positions would vary according to the results presented for Suject 'B' (Figure 6.7). Similarly, 2^{nd} and 3^{rd} Cardan angle measurements are somewhat difficult to interpret because they measure rotations about rotated axes.

7. Conclusions and Future Work

The objective of this project was to develop methods for modeling *in vivo* lumbar spine kinematics of a generalized population. Despite substantial attention from clinicians and researchers, lumbar spine biomechanics are not fully understood, as indicated by a lack of consensus regarding pathological mechanisms and clinical treatments. The methods presented here provide several distinct strengths for observing and modeling lumbar vertebral kinematics.

7.1 Study Population

Data was collected from 50 people (25 males, 25 females) performing standing flexion and extension postures using a FONAR 0.6-Tesla positional MRI scanner (Table. 7.1). All participants were healthy and had no history of low back pain or injury. The images provide gravitationally loaded vertebral configuration of the lumbar vertebrae and sacrum.

Table 7.1: Anthropometric characteristics of study population

Characteristic	**Mean**	**Minimum**	**Maximum**
Age (years)	30.4 ±7.1	19.9	44.7
Height (cm) [in]	172.3±10.5 [67.8±4.1]	156.5 [61.6]	197.5 [77.8]
Weight (kg) [lbs]	72.8±15.9 [160.2±34.9]	39.3 [86.4]	113.5 [249.8]
Body Fat (%)	18.1±8.1	3.5	36.3

Future expansion of the data set may include participants with pathological low back conditions to evaluate kinematic differences between populations.

7.2 Vertebral Reconstruction and Measurement

A novel method was developed for measuring three-dimensional vertebral position and orientation using positional MRI. Positional MRI offers a unique ability to observe bony and soft tissues in a variety of naturally loaded postures *in vivo* without exposure to ionizing radiation. However, low imaging power has previously limited the use of positional MRI because of prohibitive data processing methods and uncertain accuracy. The reconstruction and measurement method presented here is insensitive to rater error, and demonstrates improved efficiency with quantifiable accuracy. By addressing these factors, the reconstruction and measurement technique expands the capabilities of positional MRI as a biomechanical research tool and allows for compilation of statistically powered data sets.

Future development and refinement of the measurement method should address low reliability for out of plane reconstructions. One approach to improving these results may be through additional registration steps. For example, iterative closest point could be combined with an optimization technique such as simulated annealing to help ensure that the global minimum is achieved during vertebral registration. Once initial alignment convergence is achieved using ICP, simulated annealing would apply spatial-alignment perturbations to the reference vertebrae, followed by additional ICP alignment from the perturbed position.

7.3 Principal Component-based Geometric Models

Principal component regression was applied to *in vivo* measurements of lumbar vertebral position and rotation to determine manifolds that describe the full range of

vertebral motion during flexion and extension. This approach for evaluating vertebral kinematics offers several advantages compared to techniques that require *a priori* assumptions about the relationship between dependent and independent variables, such as linear regression. Principal component-based modeling preserves kinematic accuracy through direct identification of order within the measurement data, preventing occurrence of model-induced errors resulting from approximations or incorrect characterizations of biomechanical performance. Conversely, principal component-based models eliminate complexity that is not beneficial for representing system behavior through dimensionality reduction.

The results demonstrate considerable promise for further future development of principal component-based manifolds used to describe *in vivo* lumbar kinematics. Future development should expand this work to enable predictive kinematic modeling through principal component-based manifolds. This will require an appropriate goodness of fit metric that evaluates the sum of square residuals projected orthogonally onto the manifold. An information criterion, (such as Akaike's Information Criterion) is necessary for evaluating model accuracy and simplicity. Finally, cross-validation will be necessary to estimate generalization error for making predictions on subjects not included within the training data. This may be accomplished using leave-one-out cross-validation with the fully processed 50-participant data set. The model will be trained with 49 data sets and its predictive capacity evaluated on the remaining data set. Generalization error will be determined based on the prediction error using all 50 data sets.

In addition, future work may include expansion from planar position and rotation curves (1D manifolds) to three dimensional surfaces (2D manifolds) for describing

vertebral motion with three rectangular degrees of freedom. If successful, higher order spaces could be used to model full rotational and positional information (6 DoF). Principal component-based models can easily accommodate dimensionality expansion. However, robust goodness of fit measures will be necessary when evaluating the manifolds for kinematic feasibility. Visual identification methods are more susceptible to error when evaluating higher order spaces. Efforts to incorporate additional dimensionality will be contingent upon an ability to achieve satisfactory measurement results for out of plane position and orientation.

Bibliography

Adams, M. A. & Hutton, W.C., 1985. The effect of posture on the lumbar spine. *The journal of bone and joint surgery*, 67-B(4), pp.625–629.

Adams, Michael A & Roughley, P.J., 2006. What is intervertebral disc degeneration, and what causes it? *Spine*, 31(18), pp.2151–61.

Ahmadi, A. et al., 2009. Kinematic analysis of dynamic lumbar motion in patients with lumbar segmental instability using digital videofluoroscopy. *European spine journal*, 18(11), pp.1677–85.

Allbrook, D., 1957. Movements of the lumbar spinal column. *The journal of bone and joint surgery*, 39 B(2), pp.339–345.

Alyas, F., Connell, D. & Saifuddin, A., 2008. Upright positional MRI of the lumbar spine. *Clinical radiology*, 63(9), pp.1035–1048.

Andersson, G.B., 1999. Epidemiological features of chronic low-back pain. *Lancet*, 354(9178), pp.581–5.

Arjmand, N., Shirazi-Adl, A. & Parnianpour, M, 2007. Trunk biomechanical models based on equilibrium at a single-level violate equilibrium at other levels. *European spine journal*, 16(5), pp.701–9.

Aspden, R M, 1988. A new mathematical model of the spine and its relationship to spinal loading in the workplace. *Applied ergonomics*, 19(4), pp.319–23.

Bao, Q.B. et al., 1996. The artificial disc: theory, design and materials. *Biomaterials*, 17(12), pp.1157–67.

Besl, P. & McKay, N., 1992. A method for registration of 3-D shapes. *IEEE Transactions on Pattern Analysis and Machine Intelligence*, 14(2), pp.239–256.

Breiman, L., 2001. Statistical Modeling : The Two Cultures. *Statistical Science*, 16(3), pp.199–231.

Brenner, D.J. & Hall, E.J., 2007. Computed tomography--an increasing source of radiation exposure. *The New England journal of medicine*, 357(22), pp.2277–84.

Brown, M.D., Holmes, D.C. & Heiner, A.D., 2002. Measurement of cadaver lumbar spine motion segment stiffness. *Spine*, 27(9), pp.918–22.

Burdett, R.G., Brown, K.E. & Fall, M.P., 1986a. Reliability and validity of four instruments for measuring lumbar spine and pelvic positions. *Physical therapy*, 66(5), pp.677–84.

Burdett, R.G., Brown, K.E. & Fall, M.P., 1986b. Reliability and validity of four instruments for measuring lumbar spine and pelvic positions. *Physical therapy*, 66(5), pp.677–84.

Carballido-Gamio, J., Belongie, S.J. & Majumdar, S., 2004. Normalized cuts in 3-D for spinal MRI segmentation. *IEEE transactions on medical imaging*, 23(1), pp.36–44.

Cargill, S.C., Pearcy, M. & Barry, M.D., 2007. Three-dimensional lumbar spine postures measured by magnetic resonance imaging reconstruction. *Spine*, 32(11), pp.1242–8.

Chiou, W.-K. et al., 1996. A non-invasive protocol for the determination of lumbar spine mobility. *Clinical biomechanics*, 11(8), pp.474–480.

Christophy, M. et al., 2012. A musculoskeletal model for the lumbar spine. *Biomechanics and modeling in mechanobiology*, 11(1-2), pp.19–34.

Chu, C., Jenkins, O.C. & Mataric, M.J., 2003. Markerless Kinematic Model and Motion Capture from Volume Sequences. In *Proceedings of IEEE Computer Vision and Pattern Recognition*. Madison, Wisconsin, pp. 475–482.

Cornell, J.A. & Berger, R.D., 1987. Factors that Influence the Value of the Coefficient of Determination in Simple Linear and Nonlinear Regression Models. *Phytopathology*, 77(1), pp.63–70.

Deyo, R.A. et al., 1991. Cost, controversy, crisis: low back pain and the health of the public. *Annual review of public health*, 12(1), pp.141–156.

Draper, C.E. et al., 2008. Feasibility of using real-time MRI to measure joint kinematics in 1.5T and open-bore 0.5T systems. *Journal of magnetic resonance imaging*, 28(1), pp.158–66.

Dunk, N.M. et al., 2009. Evidence of a pelvis-driven flexion pattern: are the joints of the lower lumbar spine fully flexed in seated postures? *Clinical biomechanics*, 24(2), pp.164–8.

Fritz, J.M., Piva, S.R. & Childs, J.D., 2005. Accuracy of the clinical examination to predict radiographic instability of the lumbar spine. *European spine journal*, 14(8), pp.743–50.

Frobin, W. et al., 1996. Precision measurement of segmental motion from flexion-extension radiographs of the lumbar spine. *Clinical biomechanics*, 11(8), pp.457–465.

Fujii, R. et al., 2007. Kinematics of the lumbar spine in trunk rotation: in vivo three-dimensional analysis using magnetic resonance imaging. *European spine journal*, 16(11), pp.1867–74.

Galbusera, F. et al., 2008. Design concepts in lumbar total disc arthroplasty. *European spine journal*, 17(12), pp.1635–50.

Gatton, M.L. & Pearcy, M J, 1999. Kinematics and movement sequencing during flexion of the lumbar spine. *Clinical biomechanics*, 14(6), pp.376–83.

Haughton, V.M. et al., 2002. Measuring the axial rotation of lumbar vertebrae in vivo with MR imaging. *AJNR. American journal of neuroradiology*, 23(7), pp.1110–6.

Huang, S.-H. et al., 2009. Learning-based vertebra detection and iterative normalized-cut segmentation for spinal MRI. *IEEE transactions on medical imaging*, 28(10), pp.1595–605.

Izzo, R. et al., 2013. Biomechanics of the spine. Part I: Spinal stability. *European journal of radiology*, 82(1), pp.118–26.

Jinkins, J.R. et al., 2003. Upright , Weight-bearing , Dynamic-kinetic Magnetic Resonance Imaging of the Spine — Review of the First Clinical Results. *Magnetic Resonance Imaging*, 6(2), pp.55–74.

Kaigle, A.M. et al., 1992. A method for the intravital measurement of interspinous kinematics. *Journal of biomechanics*, 25(4), pp.451–456.

Kimura, S. et al., 2001. Lumbar spine disc height and curvature responses to an axial load generated by a compression device compatible with magnetic resonance imaging. *Spine*, 26(23), pp.2596–2600.

Lee, S.-U. et al., 2003. Lumbar spine disc heights and curvature: upright posture vs. supine compression harness. *Aviation, space, and environmental medicine*, 74(5), pp.512–6.

Legaspi, O. & Edmond, S.L., 2007. Does the Evidence Support the Existence of Lumbar Spine Coupled Motion? A Critical Review of the Literature. *The Journal of orthopaedic and sports physical therapy*, 37(4), pp.169–178.

Leone, A. et al., 2007. Lumbar intervertebral instability: a review. *Radiology*, 245(1), pp.62–77.

Lim, T. et al., 1997. A noninvasive, three-dimensional spinal motion analysis method. *Spine*, 22(17), pp.1996–2000.

Lin, H., 2008. Identification of spinal deformity classification with total curvature analysis and artificial neural network. *IEEE transactions on bio-medical engineering*, 55(1), pp.376–82.

Ma, H.T. et al., 2008. A new method for determining lumbar spine motion using Bayesian belief network. *Medical & biological engineering & computing*, 46(4), pp.333–40.

Maintz, J.B.A. & Viergever, M.A., 1998. A survey of medical image registration. *Medical image analysis*, 2(1), pp.1–36.

Marras, W S. & Granata, K.P., 1997. The development of an EMG-assisted model to assess spine loading during whole-body free-dynamic lifting. *Journal of electromyography and kinesiology*, 7(4), pp.259–268.

McGill, S., 1996. A revised anatomical model of the abdominal musculature for torso flexion efforts. *Journal of biomechanics*, 29(7), pp.973–977.

Meakin, J.R. et al., 2008. The effect of axial load on the sagittal plane curvature of the upright human spine in vivo. *Journal of biomechanics*, 41(13), pp.2850–4.

Mulholland, R.C., 2008. The myth of lumbar instability: the importance of abnormal loading as a cause of low back pain. *European spine journal*, 17(5), pp.619–25.

Niosi, C. a & Oxland, T.R., 2004. Degenerative mechanics of the lumbar spine. *The spine journal*, 4(6 Suppl), p.202S–208S.

Ochia, R. et al., 2006. Three-dimensional in vivo measurement of lumbar spine segmental motion. *Spine*, 31(18), pp.2073–2078.

Panjabi, M.M., 2006. A hypothesis of chronic back pain: ligament subfailure injuries lead to muscle control dysfunction. *European spine journal*, 15(5), pp.668–76.

Panjabi, M.M., 2003. Clinical spinal instability and low back pain. *Journal of electromyography and kinesiology*, 13(4), pp.371–379.

Pearcy, Mark J. & Bogduk, N., 1988. Instantaneous axes of rotation of the lumbar intervertebral joints. *Spine*, 13(9), pp.1033–1041.

Portney, L. & Watkins, M., 2000. Statistical measures of reliability. In *Foundations of clinical research*. New Jersey: Prentice Hall, pp. 557–586.

Pulli, K., 1999. Multiview registration for large data sets. *Second International Conference on 3-D Digital Imaging and Modeling (Cat. No.PR00062)*, 1, pp.160–168.

Ren, L. et al., 2005. A data-driven approach to quantifying natural human motion. In *ACM SIGGRAPH 2005*. New York, New York, USA: ACM Press, p. Paper 288.

Schmid, J. & Magnenat-Thalmann, N., 2008. MRI bone segmentation using deformable models and shape priors. *Medical image computing and computer-assisted intervention : MICCAI*, 11(Pt 1), pp.119–26.

Sicard, C. & Gagnon, M., 1993. A geometric model of the lumbar spine in the sagittal plane. *Spine*, 18(5), pp.646–658.

Simonidis, C., Scharmacher, M. & Seemann, W., 2007. Reduced kinematic model of the human spine. *PAMM*, 7(1), pp.4020025–4020026.

Splittstoesser, R.E., Knapik, G.G. & Marras, William S., 2011. A Simple Model of Changes in Lumbar Intervertebral Angles During Sagittal Torso Flexion. In *Proceedings of the Human Factors and Ergonomics Society Annual Meeting*. Las Vegas, NV, pp. 1029–1033.

Stokes, I. a F. & Iatridis, J.C., 2004. Mechanical conditions that accelerate intervertebral disc degeneration: overload versus immobilization. *Spine*, 29(23), pp.2724–32.

Strickland, C.G. et al., 2011. Development of subject-specific geometric spine model through use of automated active contour segmentation and kinematic constraint-limited registration. *Journal of digital imaging*, 24(5), pp.926–42.

Teyhen, D.S. et al., 2007. Fluoroscopic video to identify aberrant lumbar motion. *Spine*, 32(7), pp.E220–9.

Wagner, H. et al., 2012. Spinal lordosis optimizes the requirements for a stable erect posture. *Theoretical biology & medical modelling*, 9(13), pp.1–12.

Wilke, H.J. et al., 1997. Anatomy of the sheep spine and its comparison to the human spine. *The Anatomical Record*, 247(4), pp.542–55.

Wisleder, D. et al., 2001. A method to study lumbar spine response to axial compression during magnetic resonance imaging: technical note. *Spine*, 26(18), pp.E416–E420.

Wood, K. et al., 1996. Effect of patient position on the sagittal-plane profile of the thoracolumbar spine. *Journal of Spinal Disorders*, 9(2), pp.165–169.

Wu, G. & Cavanagh, P., 1995. ISB recommendations for standardization in the reporting of kinematic data. *Journal of biomechanics*, 28(10), pp.1257–1261.

Y-H, Lee et al., 1995. Predictive model of intersegmental mobility of lumbar spine in the sagittal plane from skin markers. *Clinical biomechanics*, 10(8), pp.413–420.

Zander, T., Rohlmann, A. & Bergmann, G., 2009. Influence of different artificial disc kinematics on spine biomechanics. *Clinical biomechanics*, 24(2), pp.135–42.

De Zee, M. et al., 2007. A generic detailed rigid-body lumbar spine model. *Journal of biomechanics*, 40(6), pp.1219–27.

Zhang, X. & Xiong, J., 2003. Model-guided derivation of lumbar vertebral kinematics in vivo reveals the difference between external marker-defined and internal segmental rotations. *Journal of biomechanics*, 36(1), pp.9–17.

Zou, J. et al., 2008. Missed lumbar disc herniations diagnosed with kinetic magnetic resonance imaging. *Spine*, 33(5), pp.E140–4.

Appendix: Additional Notes on Data Quality

The data presented here were processed sequentially in the order that they were collected. That is, the reliability data presented in Chapter 3 and the geometric modeling data presented in Chapter 5 represent results from the first 10 subjects that were collected. Though the data collection protocol remained consistent throughout the study, image quality improved in latter subjects (subject #26-50) through using an abdominal solenoid coil for image collection during standing flexion and extension positions. Scans collected from subjects #1-25 used a planar coil for all postures.

The planar coil is restricted in its positioning within the scanner, resulting in large object-to-image distances and reduced signal-to-noise ratio. In addition, the coil has rigid planar geometry which prevents the ability to conform to lumbar vertebral curvature during standing flexion and extension positions. This effect is most prevalent in the inferior vertebrae (L4-Sacrum) during extension postures and most prevalent in the superior vertebrae during flexion postures because the anatomy is farthest from magnetic isocenter during their respective postures (Fig A.1).

The solenoid coil is a belt that is fastened around the participant's lower abdomen, centered on the iliac crest. The solenoid coil maintains close proximity to the torso regardless of posture and improves magnetic field strength at the lumbar spine. Based on visual comparison of image quality, the results presented here for subjects #1-10 provide

a conservative estimate of reliability and accuracy that can be achieved from the latter data (collected using a solenoid coil).

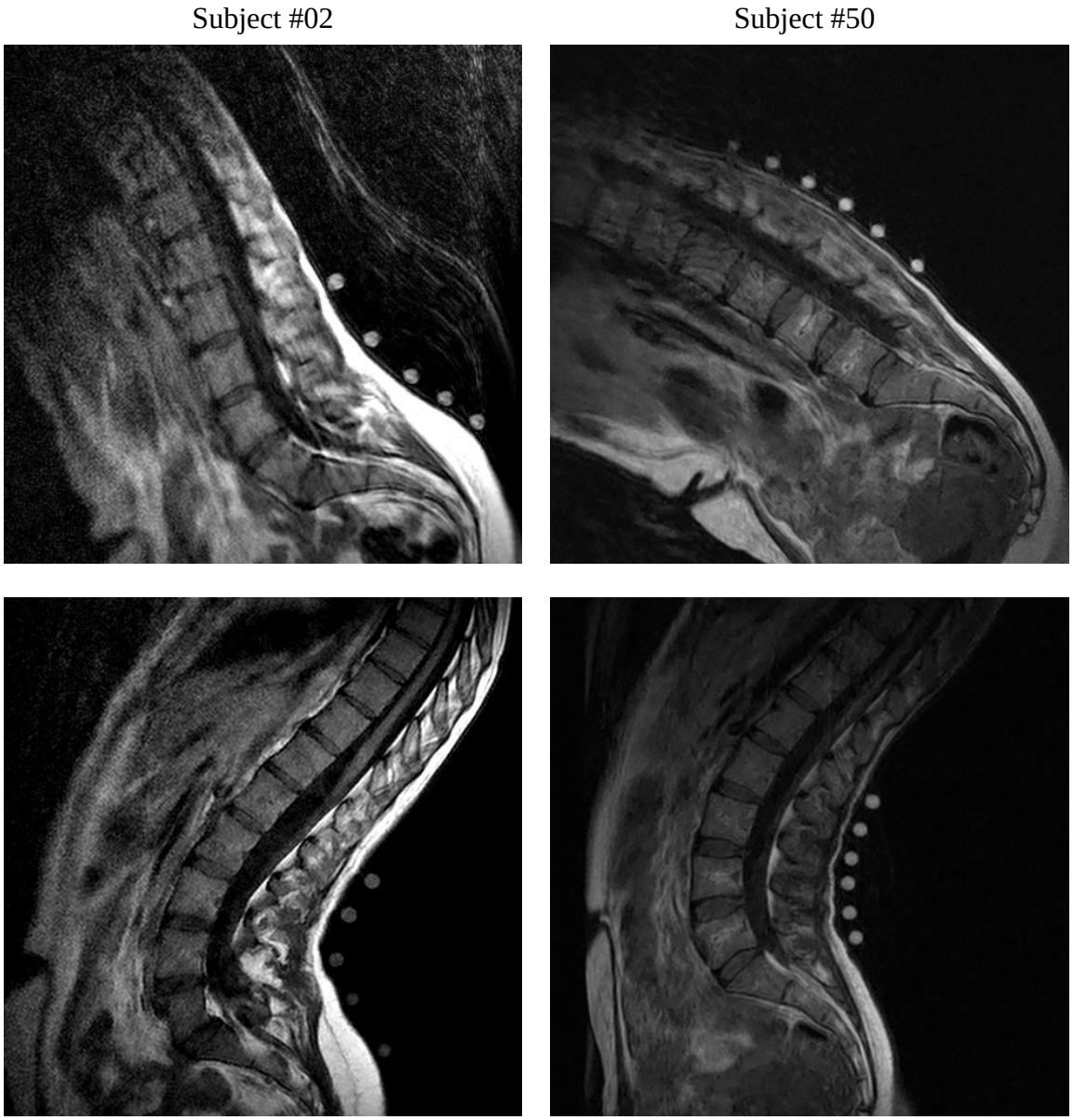

Figure A.1: Side-by-side comparison of MR images from Subject #2 (left) and Subject #50 (right), performing flexion (top) and extension (bottom) postures. Subjects #1-25 were scanned using a planar coil and subjects #26-50 were scanned using a solenoid coil fastened around the abdomen and centered at the iliac crest. The planar coil was fixed to the posterior wall of the scanner, resulting in increased object-to-image distance and reduced image quality during standing postures. This effect is most apparent in the superior lumbar spine during flexion and in the inferior lumbar spine during extension postures due to increased distance from the posterior scanner wall. By comparison, the solenoid coil produces more uniform scans with greater image clarity, as indicated by a well-defined boundaries between bone and the surrounding soft tissues.